A Comprehensive Review on Barium Titanate Nanoparticles as a Persuasive Piezoelectric Material for Biomedical Applications: Prospects and Challenges

Ankur Sood, Margaux Desseigne, Atul Dev, Lionel Maurizi, Anuj Kumar, Nadine Millot, Sung Soo Han

A Comprehensive Review on Barium titanate Nanoparticles as a Persuasive Piezoelectric Material for Biomedical Applications: Prospects and Challenges

Ankur Sood[1], Margaux Desseigne[2], Atul Dev[3], Lionel Maurizi[2], Anuj Kumar[1,4*], Nadine Millot[2*], Sung Soo Han[1,4*]

[1] *School of Chemical Engineering, Yeungnam University, 280 Daehak-ro, Gyeongsan 38541, South Korea*

[2] *Laboratoire Interdisciplinaire Carnot de Bourgogne, UMR 6303 CNRS / Université Bourgogne Franche-Comté, 9 Avenue Alain Savary, BP 47870, 21078 Dijon, France*

[3] *Division of Gastroenterology & Hepatology, School of Medicine, Institute for Regenerative Cures, University of California Davis, 2921 Stockton Boulevard, Sacramento, CA 95817, USA*

[4] *Institute of Cell Culture, Yeungnam University, 280 Daehak-ro, Gyeongsan 38541, South Korea*

Correspondence: **nadine.millot@u-bourgogne.fr** (N.M.), **sshan@yu.ac.kr** (S.S.H.), **anuj.budhera@gmail.com** (A.K.)

Abstract

Stimulation of cells with electrical cues is an imperative approach to interact with biological

systems and has been exploited in clinical practices over a wide range of pathological ailments. This bioelectric interface has been extensively explored with the help of piezoelectric materials, leading to remarkable advancement in the past two decades. Among other members of this fraternity, colloidal perovskite barium titanate ($BaTiO_3$) have gained substantial interest due to their noteworthy properties which includes high dielectric constant, and excellent ferroelectric properties along with acceptable biocompatibility. Significant progression is witnessed for $BaTiO_3$ nanoparticles ($BaTiO_3$ NPs) as a potent candidate for biomedical applications and in wearable bioelectronics making it a promising personal healthcare platform. The current review highlights the nanostructured piezoelectric bio interface of $BaTiO_3$ NPs in applications comprising drug delivery, tissue engineering, bioimaging, bioelectronics and wearable devices. A particular attention has been dedicated towards the fabrication routes of $BaTiO_3$ NPs along with different approaches for its surface modifications. The review offers a comprehensive discussion on the utility of $BaTiO_3$ NPs as active devices rather than passive structural unit behaving as carriers for biomolecules. The employment of $BaTiO_3$ NPs presents new scenarios and opportunity in the vast field of nanomedicines for biomedical applications.

Key words: Barium titanate; piezoelectricity, nanoparticles, biomedical, bioelectronics

1. Introduction

Biological systems are a complex architect with a continuously enduring succession of

concurrent events leading to numerous biochemical responses. Appropriateness of a material for biomedical applications is substantially concluded by their extent of interaction with the biological system. A variety of organic and inorganic nanoparticles has been demonstrated to interact with biological systems which includes metal oxide [1-4], magnetic materials [5-7], noble metals [8], polymeric particles [9, 10], miscellaneous inorganic compounds [11-13] *etc.* Recently, a lot of emphasis has been given to piezoelectric nanomaterials, which are known to become electrically polarized under mechanical stress. This feature plays a crucial role in muscle and nerve cells in generating and propagating the action potentials across nerves and muscles [14]. Endogenous electric field (EEFs) is also critical in controlling other cellular physiology and functions, including differentiation, proliferation, migration, morphology, and gene expression [15]. In addition, EEFs also influence cell division, intracellular interaction, ion transport, mechanotransduction, nervous system along with its accountability in bone and skin tissues healing [16, 17]. Bioelectricity is an essential part of living system and plays a crucial role in the early embryonic stage as developmental defects may arise due to minor deviations from the steady-state potential of the embryo [18, 19].

Up recently, the piezoelectric properties of materials have been exploited to provide interfaces with biological systems [20, 21]. Electrically stimulating cells/tissues has been an imperative approach in order to interact with living matter and has been explored for clinical practice in case of many pathological ailments [22]. However, the orthodox method of simulation often requires installation of implanted electrodes and wired networks. Therefore, the opportunity to achieve indirect electrical simulation through mechanically driven methodology using piezoelectric materials is of great interest [20]. Wireless stimulation of tissues has not only been

exploited for the treatment of many ailments [23-25] but has also been investigated in the field of tissue engineering or regenerative medicine where electrical stimulation is a regulatory step in the alteration of the functions of a tissue [26, 27].

Piezoelectricity is offered by both organic and inorganic materials where the rationale of piezoelectricity is influenced by the category of material. In case of organic materials, upon induction of mechanical stress, the electric polarization is induced by reorientation of molecular dipole. In contrast, the piezoelectric effect in inorganic materials mainly evolves as a result of the rearrangement of ions in the dielectric materials deficient of inversion symmetry in their crystalline structure [28, 29].

In the league of inorganic piezoelectric materials, zinc oxide (ZnO) [30, 31], and boron nitride (BN) [32, 33] have been widely studied for their biomedical applications, even if ZnO toxicity is now well-known [34, 35]. Up recently, ceramic nanomaterials based on perovskite-like oxides have attracted the interest of many research groups for their utility in biomedical applications [36, 37]. With high dielectric constant, and excellent ferroelectric properties, barium titanate ($BaTiO_3$) is perhaps one of the most studied compounds of the perovskite family. Biocompatibility, piezoelectric properties, and non-linear optical features are some of the advantages offered by this fascinating material which could be explored for its applicability in different biomedical applications [38]. Notably, recent reports suggest that $BaTiO_3$ NPs could be used in a wide range of biomedical applications, including non-linear imaging purposes, drug delivery, tissue engineering, and bio-stimulation [39-41]. Although, it is reported that the nonlinear efficiency of most inorganic nanocrystals ($BaTiO_3$, ZnO, $KTiOPO_4$, $LiNbO_3$, $KNbO_3$) used for developing harmonic nanoparticles are similar [42] but for biomedical application, the

biocompatibility has always been marked as an essential requirement. Dantec *et al.* studied the nonlinear optical properties of ZnO and $BaTiO_3$ individually, and based on the analysis marked them as one of the most promising second harmonic probes for imaging applications [43]. Further, the superiority of $BaTiO_3$ in terms of frequency response and power generation has also been reported in comparison to ZnO and barium sodium niobite (BNN) [44]. With a wide range of inorganic nanomaterials investigated in the field of biomedicine, the potency of $BaTiO_3$ NPs is not sufficiently explored.

Some reviews have already highlighted the importance of $BaTiO_3$ NPs, among them the review by Genchi *et al*. summarizes the utility of $BaTiO_3$ NPs as smart nanomaterials for nanomedicines with much emphasize the utility as nanotransducer for cells and in tissue engineering [38]. However, this review did not highlight the applications concerning drug delivery, gene delivery, cancer therapy *etc*. Another review by Kapat *et al.* provided an overview of piezoelectric nano-biomaterials with much emphasizes on the classification of piezoelectric materials and their intrinsic properties (biopiezoelectricity) [19]. Here, the review comprehensively describes the utility of $BaTiO_3$ NPs in tissue regeneration but not much emphasize on wearable electronics and cancer therapeutics is given. Another review by Jarkov *et al.* provides some critical overview of piezoelectric materials but not totally concerns the utilization of $BaTiO_3$ NPs in biomedical applications [45]. All these reviews do not provide much details on the in depth understanding of the $BaTiO_3$ NPs cellular response along with different synthetic routes and functionalization strategies of $BaTiO_3$ NPs.

The rapid development and functionality of $BaTiO_3$ NPs in biomedical applications calls for a comprehensive review that can offer an informative reference for researchers working in

relevant fields. The current review provides a thorough overview of $BaTiO_3$ NPs from a broad perspective, with a focus on their biochemical attributes and utility in biomedical applications **(Figure 1)**. Herein, we systematically outline the representative mechanism and morphological features of $BaTiO_3$ NPs, with an emphasis on their structural aspects. The review provides a comprehensive sketch on the synthesis process of $BaTiO_3$ NPs along with its hybrids/composites accompanied by their surface modifications. The latest utilization of $BaTiO_3$ NPs in biomedical applications including drug delivery, tissue engineering, biosensing, and wearable bioelectronics are summarized. The review also highlights the efforts that could be incorporated to improve the applicability and performance of $BaTiO_3$ NPs in biomedical areas. Finally, the review is concluded with a profound analysis on the challenges that need to be addressed for practical application of this fascinating material.

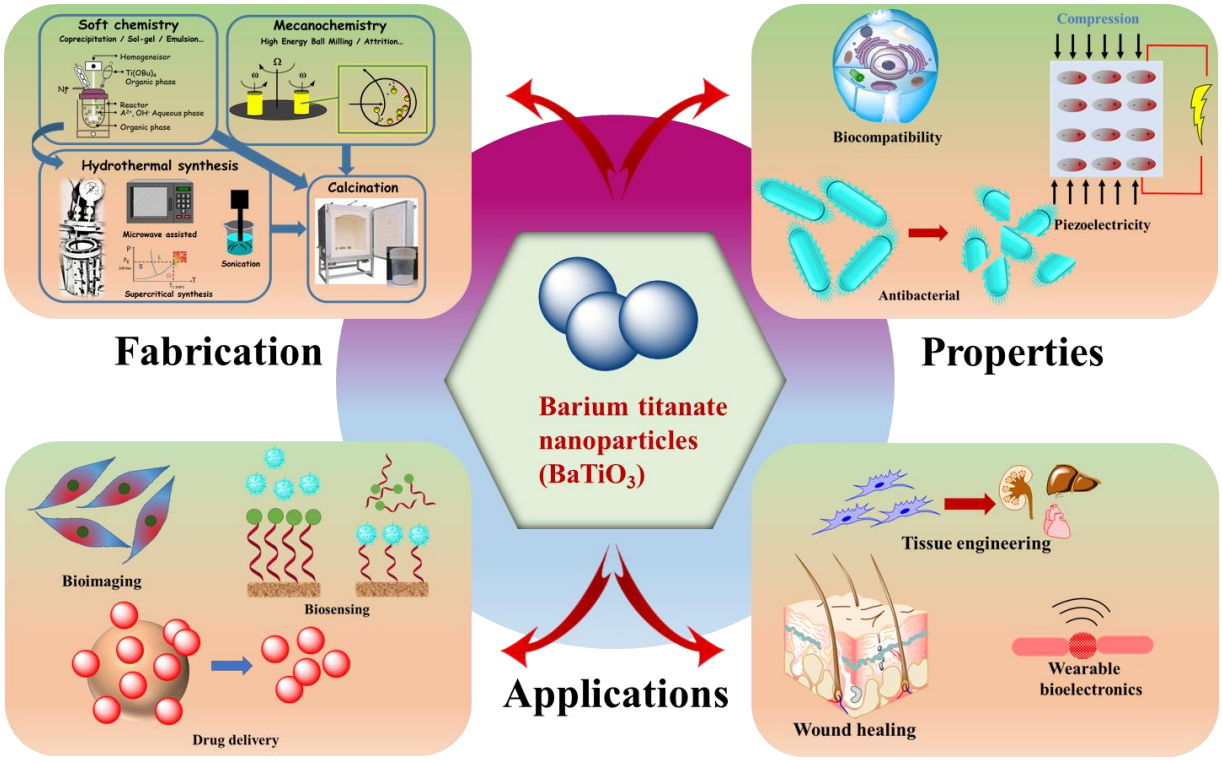

Figure 1. Schematic representation of an overview of different aspects of barium titanate nanoparticles.

2. Barium titanate ($BaTiO_3$) NPs

2.1 History and physico-chemistry of $BaTiO_3$

$BaTiO_3$ was first discovered by Wainer and Salomon in United States in 1941 during the World War II [46]. It was due to the high demand of the compact capacitors/condensers for the radar systems and based on widely used titania condenser (TiO_2-MgO), researchers doped various oxides (CaO, SrO and BaO) in wide fraction to develop materials with higher permittivity [47]. Among the series of materials, the maximum permittivity was achieved for $BaTiO_3$, which weighed ten times higher than titania at that time. Originally, $BaTiO_3$ was discovered for its

permittivity and later characterized for its high dielectric constant [48], and ferroelectricity properties [49, 50]. It was Gray at Erie Resistor [51] and Shepard Roberts at MIT [52] who showed that the electrically poled $BaTiO_3$ exhibit 'piezoelectricity' due to its domain realignment. Lately, Rooks [53] established the perovskite cubic cell crystal structure of $BaTiO_3$ with Megaw [54] providing the data to further determine its structure.

Perovskite crystal structure of $BaTiO_3$

A perovskite name adopted from a mineral perovskite ($CaTiO_3$) for the compounds which share a chemical formula ABO_3, where 'A' and 'B' represent cations and O is an anion. $BaTiO_3$ is a member of perovskite family which show perovskite crystal structure below 1460 °C and appears non-perovskite hexagonal polymorph at higher temperatures. The $BaTiO_3$ has a primitive cubic cell crystal structure with the larger cation-A [monovalent, (Ba^{2+}) divalent, or trivalent metal] in the corner, smaller cation-B [pentavalent, (Ti^{4+}) tetravalent, or trivalent element] in the middle of the cube, and the anion, commonly oxygen, in the center of the face. The perovskite structure can be considered as a 3-D framework of TiO_6 octahedra while Ba^{+2} has a coordination number of 12 [55].

Structural phase transitions in barium titanate

$BaTiO_3$ is known for temperature dependent phase transitions of its crystal structure, below -90 °C (183 K) it acquires ferroelectric rhombohedral (R3m) crystal structure with Ti displacements aligned along a body diagonal (111). Between -90 °C and 5 °C (278 K), $BaTiO_3$ is ferroelectric orthorhombic (Amm_2) with net polarization along a face diagonal (011). Between 5 °C and 120 °C (393 K), it is ferroelectric tetragonal (P4mm) with polarization along

the z axis (001). Above 120 °C, $BaTiO_3$ become paraelectric, and show cubic (Pm3m) crystal structure **(Figure 2)** [56].

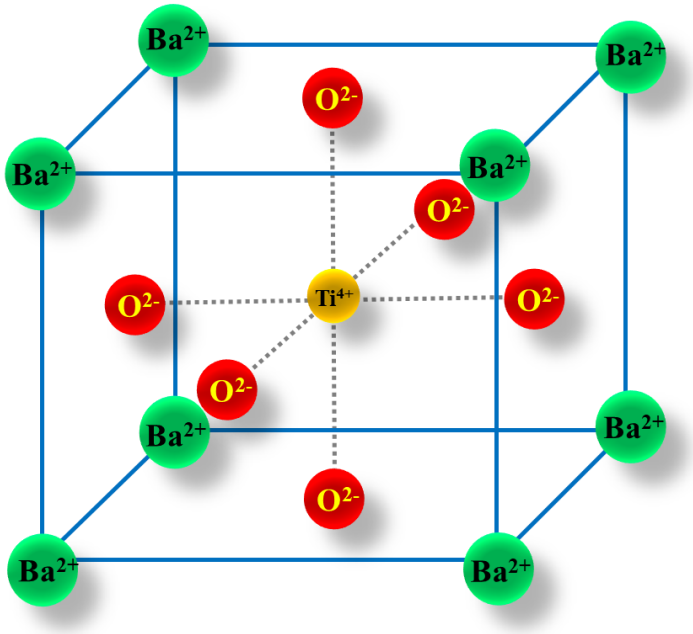

Figure 2. Crystal structure of cubic $BaTiO_3$ phase

Moreover, it is very well known that physical properties (electrical, mechanical, dielectric) of polycrystalline materials are related to the grain sizes. Phase transitions which depend on grain size induce very interesting properties in materials. The case of barium titanate is undoubtedly one of the more explored and exploited [57, 58]. It is typically demonstrated that upon reduction of the grain size of polycrystalline $BaTiO_3$ to the micron dimension, an increment in the dielectric constant is observed at room temperature. However, below the Curie temperature (Tc) substantial modification in terms of temperature dependence of the dielectric constant was observed [59-62]. In case of materials with grain size ≥ 1µm, formation of a polydomain subgrain structure is observed upon cooling (130 °C) as a result of cubic-tetragonal transformation in

order to curtail electrostatic and elastic energies in the polar anisotropic state [57]. Above the Tc (<130 °C), $BaTiO_3$ presents paraelectric behavior with cubic arrangement however, below this temperature, the structure is partially distorted with the existence of three temperature dependent ferroelectric polymorphs having nonzero dipole moment. Between 10 °C and 130 °C, the tetragonal transformation is stable whereas, below 10 °C the structure changes to orthorhombic which further transforms to rhombohedral structure below -80 °C **(Figure 3)** [63-65].

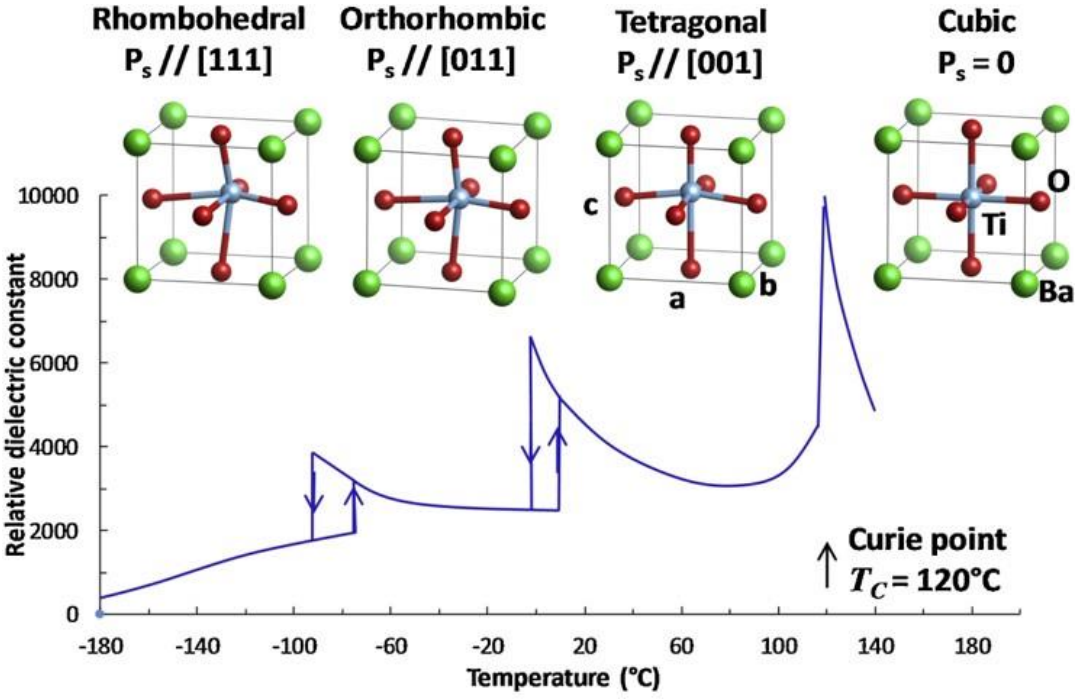

Figure 3 Evolution of crystal structure and relative dielectric constant as a function of temperature in $BaTiO_3$ single crystal. Reproduced with permission. [65] Copyright 2020, Elsevier.

A diminution of tetragonal distortion, heat of transition, Tc and relative dielectric constant has been observed on dense $BaTiO_3$ ceramics with grain size reducing from 1200 to 50 nm. It has been established that variations in the grain size/temperature/external stress modify the spontaneous polarization due to alterations of the tetragonal strain which in turn effects the phase transitions and has influence over the ferroelectric properties [66]. The size dependency of ferroelectric properties in case of isolated particles has been estimated with the help of theoretical models of the Landau-Ginsburg-Devonshire theory [67]. The critical grain size linked to the suppression of ferroelectric behavior was estimated to be 10-30 nm with the permittivity of $BaTiO_3$ of grain size < 500 nm presenting high sensitivity towards the existence of a low permittivity, and nonferroelectric grain boundary layer [66, 68].

2.2 Synthesis routes and applications of $BaTiO_3$ NPs

Different physical and chemical process were developed to synthesize zero-dimensional (0 D) and one-dimensional (1 D) $BaTiO_3$ NPs of various size and morphology. These different methods of synthesis and parameters highly govern the property of the $BaTiO_3$ NPs. Common synthetic processes involved hydrothermal methods [69-73], solvothermal [74], and sol-gel methods [75, 76] as well as co-precipitation methods with oxalates [77-79] and catecholates [80]. The main challenges of $BaTiO_3$ NPs synthesis are controlling the size and the crystalline phase to achieve desired properties. $BaTiO_3$ NPs show excellent photorefractive and ferroelectric properties and these properties have been widely used in the material science and engineering applications. However, their use in biological and medical applications has been recently explored. It has been discovered that this material could be used for *in vitro* imaging [81, 82], cell targeting [83], drug delivery [84], and nanotransducer application in biological system [85, 86].

Their piezoelectric properties could be used to provide electromechanical stimulation to the cells, which help modulate the cellular behavior under diseased conditions. This property is highly utilized in tissue engineering and regenerative medicine application at very high scale [87]. The synthesis methods and application are described in details in the later sections of this review.

2.3 Morphologies and properties of $BaTiO_3$ NPs

All the material in their nanoscale behaves differently than their bulk counterparts and $BaTiO_3$ is no exception to this. As the bulk $BaTiO_3$ NPs show high permittivity, ferroelectricity and piezoelectricity, their dielectric and ferroelectric properties heavily depend on their crystal size at nanoscale (the so-called size effect). These properties have been exploited in a wide range of applications for non-volatile random-access memory, transducers, gate dielectric, nonlinear optics, *etc.* To date, a variety of $BaTiO_3$ nanostructures of various size and morphology including nanodots [88, 89], nanoparticles [90], nanobowls [91], nanowires [92], nanocubes [93] and nanorods [94] have been developed in different crystalline phases (*e.g.*, cubic, tetragonal, or multi-crystalline). A reduction in the size of the material to the nanoscale significantly affects dipoles length in the $BaTiO_3$ crystal structure and lead to the unique dielectric and ferroelectric properties. Their microstructures, composition, applied stress, defect concentration and surface composition further contribute to the unique properties in their nanoform [85]. Therefore, understanding of phase design and its manipulation at the nanoscale is of high importance to develop micro and nano devices that rely on dielectric and ferromagnetic properties of the material. Dielectric properties show a strong correlation with particle size. Initially, dielectric constant of the material increases to a maximum value with successive decrease in the particle

size, however, further decrease in particle size results in decline in its dielectric constant [95, 96]. The ferroelectric Tc of 0 D $BaTiO_3$ NPs decreases progressively with size, resulting in room temperature stabilization of the paraelectric cubic phase while 1 D $BaTiO_3$ nanowires of 10 nm diameter still retain their ferroelectric properties. A recent study has suggested that ferroelectricity is present in all form of $BaTiO_3$ NPs regardless of their size and the density of these is a function of particle morphology [97, 98]. Compared to 0 D, 1 D nanostructures of $BaTiO_3$ are highly influenced by extrinsic strains generated during the fabrication process. Depending upon the type of strain produced can either enhance or suppress the polarization [99]. In a recent study, phase field simulation was used to analyze the relationship between ceramic morphology and output performance of piezoelectric nanocomposites [100]. Ferroelectricity is defined as the property of spontaneous electrical polarization under the influence of an external electric field. This switchable polarization is ideal for the development of microelectronics and is highly influenced by the surface effect. Atomic or molecular adsorbates including surface ligands [101, 102] and coatings [103] stabilize the ferroelectricity of nanoscale $BaTiO_3$ and make it useful to design ferroelectric devices that can operate at the atomic scale. High performance $BaTiO_3$ nanocomposite materials have been prepared by integrating complementary polymers (polyvinylidene fluoride (PVDF) [104, 105], polyacrylamide (PAmA) [106, 107], poly(2-hydroxylethyl methacrylate) (PHFDA) [108] , poly (vinylidene fluoride - hexafluoro propylene) (P(VDF–HFP)) [109, 110], 2-[2-(2-methoxyethoxy) ethoxy]ethyl} phosphonic acid (PEGPA) [102, 111] with $BaTiO_3$. These nanocomposites offer superior performance, processability and scalability than the pure $BaTiO_3$ nanostructures.

2.4 Antibacterial and biological response of $BaTiO_3$

The potential of $BaTiO_3$ as a compelling candidate for various biomedical applications has been reported by many research groups [112, 113]. In addition to the dielectric and ferroelectric properties, researchers have also reported the antimicrobial properties of $BaTiO_3$. Metal based nanoparticles when interact with high energy light beams produce Reactive Oxygen Species (ROS) and this property could be utilized to develop new generation antimicrobial agents. In a study reported by Shah *et al.*, $BaTiO_3$ NPs (~ 100 nm) were prepared by co-precipitation method using barium nitrate, titanium dioxide, and oxalic acid as the precursors and evaluated for their antimicrobial efficacy against the human pathogenic bacteria. Through this work, $BaTiO_3$ NPs have demonstrated a dose dependent significant reduction in gram-positive and gram-negative bacterial growth and have pronounced effect on the biofilm formation against clinical isolates of P. *aeruginosa* and S. *aureus*. at a very low concentration [114]. In an independent study, Sasikumar *et al*, studied the antimicrobial activity of hydrothermally synthesized cubic shaped $BaTiO_3$ NPs. These NPs have shown antimicrobial activity against various multidrug-resistant pathogens and *C. albicans* at very low dose. These antimicrobial activities are attributed to the decrease in ergosterol biosynthesis in *C. albicans* [115]. $BaTiO_3$ NPs shows both bactericidal and bacteriostatic properties which was evaluated by Francesco Boschetto *et al.* in a study where they incorporated $BaTiO_3$ NPs in the Polylactic acid (PLA) fibres produced by centrifugal spinning to improve their bacteriostatic behavior. The PLA coated $BaTiO_3$ NPs have shown dose dependent response on the growth of *Staphylococcus epidermidis* [116]. In addition to the antimicrobial properties, there have been reports on the biological responses of $BaTiO_3$ NPs which is dependent on the size and surface properties of

the fabricated nanoparticles. $BaTiO_3$ NPs are susceptible to produce oxidative stress in the cancerous cells as reported by Ahamed *et al.* by studying the interaction of $BaTiO_3$ NPs with human lung carcinoma (A549) cells [117]. The study reported the oxidative stress mediated, dose and time dependent cytotoxicity upon interaction of the cells with $BaTiO_3$ NPs together with diminution of mitochondrial membrane potential and stimulation of related enzymatic activity (caspase-3/-9). Here, the oxidative stress was induced due to production of pro-oxidants (ROS and H_2O_2) and decline of antioxidants (glutathione). On similar grounds, Candito *et al.* studied the antioxidant properties of $BaTiO_3$ NPs on neural cell line, PC12 where its biological responses were analyzed through studies concerning cell viability, cell morphology, apoptotic markers, oxidative stress and neurite outgrowth [118].

Since inception for laser, nonlinear optics have been significantly developed and have been an active research area [119, 120]. There are different non-linear optical effects of which the second harmonic generation (SHG) has gained substantial attraction globally. SHG is a parametric nonlinear process in which two photons with the same frequency interact with a nonlinear optical material and emitting another photon with double the frequency [121]. Over the past two decades, nanomaterials have been explored for their optical non-linearity, due to their local field effect which results in their enhanced non-linear optical responses [122, 123]. In case of mid-refractive all dielectric nanomaterial (e.g. $BaTiO_3$ NPs), the electric and magnetic dipole resonances are spectrally coinciding, enhancing the electromagnetic fields over a wide spectral range [124]. Therefore, $BaTiO_3$ NPs have been explored as a potent harmonic nanoprobes/contrast agent for non-linear bioimaging applications and have shown great potential for sustainable, tunable, coherent and biocompatible imaging [125, 126].

Barium has also been highlighted as contrast agents for computed tomography (CT) with predominantly barium sulfate ($BaSO_4$) suspension has been explored for enhanced CT contrast in imaging gastrointestinal tract [127]. Barium has a high atomic number (Z) due to which the photon energy corresponding to highest attenuation stage of barium overlaps with the X-ray energy distribution peak produced by clinical CT scanners, thus absorbing more photons than any other element [128]. Even with such a remarkable CT contrast potential, high toxicity restricts the use of barium-based materials as a CT contrast agent however, recently, studies have been underway to explore the use of $BaTiO_3$ NPs as CT contrast agent due to its high biocompatibility and ease of surface modifications [127]. This high atomic number of barium could also be explored for their utility in hyperthermia treatment in destroying cancerous cells [129].

Up recently, magnetoelectric (ME) core-shell NPs have been used as a very promising drug nanocarrier for selective penetration of drugs on a specific cell resident [130, 131]. Here, the quantum coupling between ferromagnetic and ferroelectric phases produces strain mediated ME effect responsible for interaction with biological cells. Due to non-zero magnetic moment, ME NPs have control over drug delivery and drug release mechanisms by using alternative/direct current magnetic fields [132, 133]. Magnetoelectric materials tend to control the surrounding electric field, a feature linked to the cell membrane. This enables the opening of membrane pores and ingestion of nanoparticles, a prerequisite in drug delivery strategies [134]. An additional advantage of using magnetoelectric NPs is their specificity towards cancer cells through their capability of discriminating between cancerous cells and normal owing to the difference in the threshold field which is lower for cancerous cells (~ 3 mT) and higher in case

of normal cells (≥ 20 mT), enabling their specificity towards cancer cells [135].

The biological response of nanoparticles plays a significant role in their utility as a candidate for biomedical applications and can be acknowledged as the foremost requirement for their clinical translation. $BaTiO_3$ NPs have been reported to be highly biocompatible with negligible cytotoxicity to living cells. Functionalization and surface modification have been a straightforward approach used by researchers worldwide, in order to provide specificity and selectivity across biological systems [136]. Further, response against external stimulus have also been an attractive alternative, that could be incorporated in order to further improve the biological responses of $BaTiO_3$ NPs. The biological response of any material depends on both intrinsic as well as extrinsic factors. Size and shapes play an important role in the nanoparticle's internalization: different types of endocytosis are possible (phagocytosis, pinocytosis, receptor-mediated cytosis *etc.*) [137] or diffusion also called translocation [138]. Moreover, the cellular behavior is also dependent upon the surface charge on the nanoparticles along with the structural anatomy and arrangement of ions in the lattice structure which also has remarkable influence on the biological response of the nanomaterials under investigation. Finally, that is also the so-called protein corona which plays a major role when nanoparticles are investigated *in vitro* or *in vivo* [139].

3. Synthesis and functionalization of $BaTiO_3$ NPs

3.1 Different synthesis methods of $BaTiO_3$ NPs

Solid-state reaction, carried out at temperature higher than 1000 °C is a low-cost process suitable for mass production, but it is not appropriate to obtain nanoparticles. Indeed, diffusion

of atoms at such temperature leads to grain growth, allowing to reduce the surface energy of the powder. Solid-state reaction leads also to powders with low purity and large grain size distribution. Traditionally, $BaTiO_3$ NPs are prepared by solid-state reaction between $BaCO_3$ and TiO_2 under high temperature. After the oil shocks of 1973, other techniques less costly in energy and without the previous drawbacks were born, among them soft-chemistry and high-energy ball-milling.

Nowadays, $BaTiO_3$ NPs can be produced through several synthetic routes such as co-precipitation [140-146], sol-gel methods [89, 147-152], hydrothermal [146, 150, 153-159] and solvothermal [160] synthesis, and high-energy milling [144] [161-167] **(Figure 4)**.

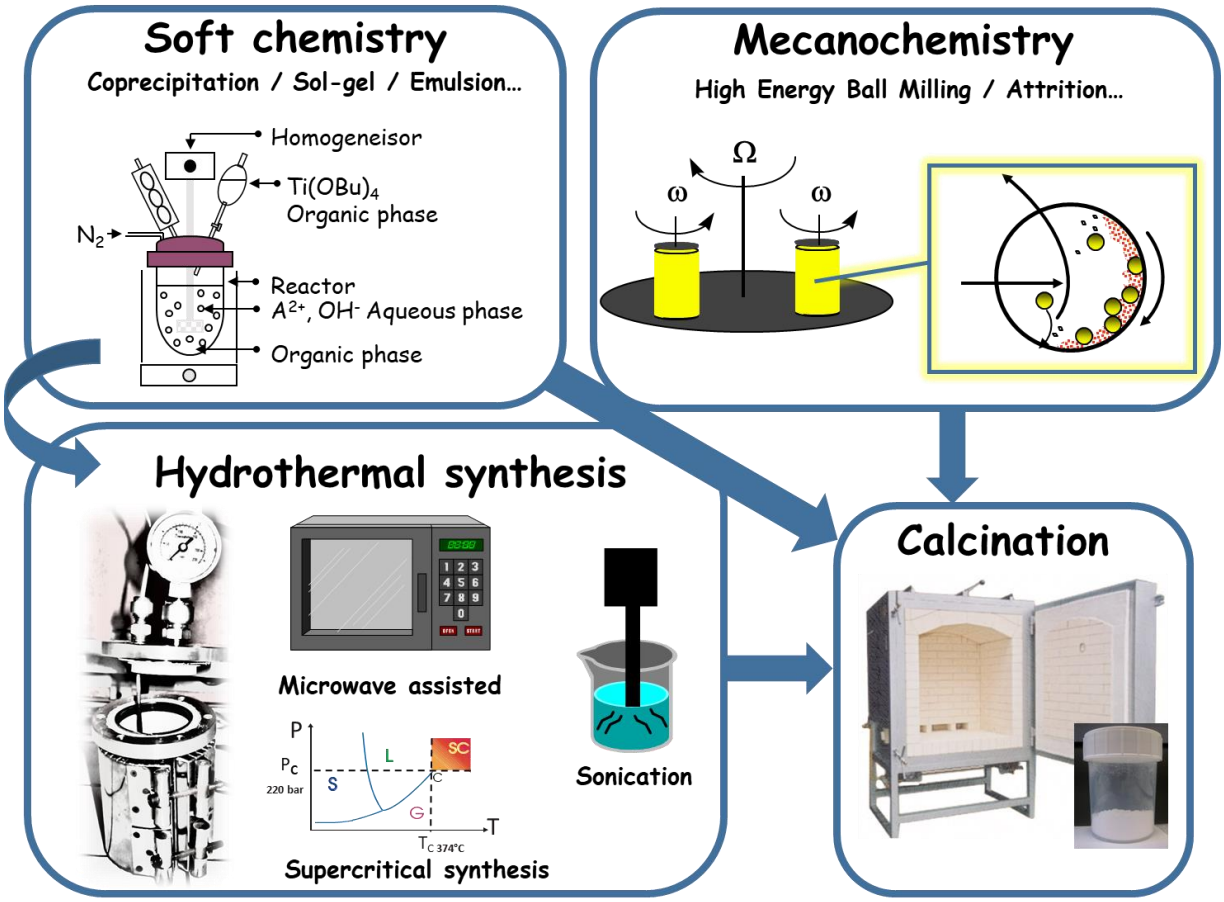

Figure 4. Schematic representation of different synthesis routes for the production of $BaTiO_3$ NPs

Other approaches are, for instance, electrochemical synthesis [150], pyrolysis [168], organometallic approach, templating [169] and electrospinning [170] or combinations of the previously mentioned methods. Further thermal treatments (at 800-1000 °C) may be required, usually to convert cubic into tetragonal $BaTiO_3$ NPs [142-144, 147, 156, 161, 166]. They are necessary in the case of the sol-gel approach. They also allow to eliminate $BaCO_3$ often present in the as-prepared samples [140].

The main challenges of $BaTiO_3$ NPs synthesis are to control several parameters: their size, the crystalline phase (cubic, tetragonal, orthorhombic *etc.*), the morphology, the surface chemistry (some examples of syntheses and powders obtained are given in **Figure 5** and, for biomedical applications, the agglomeration state while avoiding undesired by-products of reaction such as carbonates [38].

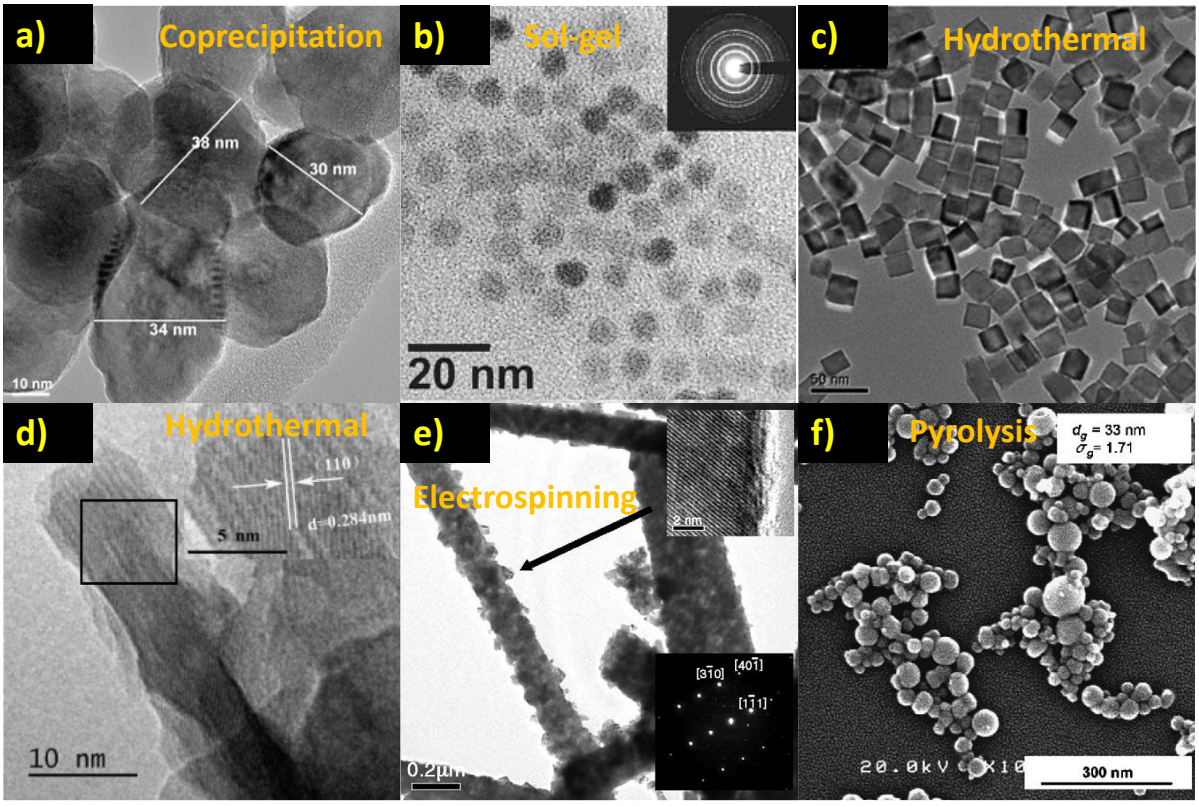

Figure 5. Different morphologies and sizes of $BaTiO_3$ obtained *via* different synthesis' routes: a), c), d), e) and f) Reproduced from publications [171], [157], [154], [170], [168] with permission from Elsevier; b) Reproduced with permission. [89] Copyright 2001, American Chemical Society.

3.1.1 Coprecipitation

Coprecipitation is the easier way to prepare NPs. Starting from cations dissolved in water, the addition of a base lead to the nucleation, then growth of NPs. The reaction involved is the following (Eq. 1):

$$BaCl_{2(aq)} + TiCl_{4(l)} + 6\ NaOH_{(aq)} \rightarrow BaTiO_{3(S\downarrow)} + 6\ NaCl_{(aq)} + 3\ H_2O \quad \textbf{Eq. 1}$$

Several variations in this synthesis process exist such as direct synthesis from solution (DSS) method. Exploring this approach, Qi *et al.* [140] obtained $BaTiO_3$ NPs using $Ba(OH)_2.8H_2O$ and tetrabutyl titanate as starting materials. Samples were dried at 65 °C for 24 h to form $BaTiO_3$ NPs. Further, Song *et al.* [145] obtained $BaTiO_3$ NPs by a continuous high-gravity reactive preparation (HGRP) technique, powders are then annealed at 900 °C for 2 h. The $BaCl_2$, $TiCl_4$ and NaOH solutions were simultaneously and continuously pumped from their storage reservoirs into different distributors in the Rotating Packed Bed machine (RPB). This apparatus provided intense mixing for the reaction. The $BaTiO_3$ NPs produced by the HGRP technique reveal a cubic structure at room temperature and a quasi-spherical morphology with a primary particle size around 90 nm. Clabaugh precipitation is also an alternative, starting from barium chloride and titanium oxychloride and using oxalic acid ; F. Baeten *et al.* [142] obtained $BaTiO_3$ NPs after annealing of the barium titanyl oxalate precursor at 1000 °C. Moreover, sonochemical approach allows to obtain highly pure powder at a lower processing temperature of about 50 °C, in contrast to 900 °C necessary for the synthesis by the mechanochemical approach [144].

Sol-gel approach was also used to produce core-shell nanoparticles of $Co_{1-x}Ni_xFe_2O_3@BaTiO_3$

[148]. The ferrite cores were obtained via classical coprecipitation at 70 °C for one hour before being calcinated at 500 °C for one more hour. $BaTiO_3$ shells were grown in an emulsion of water (with Ba precursor) and ethanolic solution (with Ti precursor). The NPs obtained are between 50 and 100 nm with quasi-spherical shapes. Combination of these two materials led to anomalous behavior in their magnetization certainly due magnetoelectric coupling of the NPs. The authors concluded by the need to further investigate this interesting phenomenon.

Co-precipitation method is a simple and well-used approach to produce metallic oxide NPs [172]. In the case of barium titanate, polydisperse nanoparticles are usually obtained that might be an issue in some applications. Furthermore, thermal treatments following co-precipitation is leading to agglomeration and impurities despite high gravity reactive routes were also developed to fix these disadvantages [145, 146].

3.1.2 Sol-gel method

In this process, metal alkoxide are first hydrolyzed and polymerized to form gels, and then annealing is used to obtain $BaTiO_3$ NPs with high purity. In the synthesis developed by S. O'Brien *et al.*, monodisperse $BaTiO_3$ NPs with diameters ranging from 6 to 12 nm were obtained thanks to a sol-gel procedure. A single bimetallic alkoxide molecular precursor is used to ensure the correct stoichiometry of the product [89]. Oleic acid was used as a stabilizing agent and the reaction occurred at 140 °C under argon or nitrogen. The absence of water prevents the premature hydrolysis of the molecular precursor. The mixture was cooled to 100 °C and hydrogen peroxide solution was injected through a septum. The solution was maintained in a close system and stirred at 100 °C for 48 h to promote hydrolysis and crystallization of the

product in an inverse micelle condition.

Pechini process is an alternative. An aqueous solution of suitable salts is mixed with an alpha-hydroxycarboxylic acid usually citric acid. Chelation takes place in the solution. A polyhydroxy alcohol is then added, and the liquid is heated above 150 °C to allow the chelates polymerization. Thermal annealing allowed to remove water and obtain the mixed oxide. L.R. Prado [150] reached a $BaTiO_3$ particles size of 44 ± 15 nm by using citric acid, barium acetate, titanium isopropoxide, ethylene glycol and NH_4OH as precursors. This solution was calcined for 5 h at 600 °C under a heating rate of 2 °C min^{-1}. A combination of sol-gel and hydrothermal treatment is also possible. Zanfir *et al.* [171], starting from tetrabutyltitanate and barium acetate, obtained average crystallite size smaller than 50 nm and a cubic symmetry for $BaTiO_3$ NPs. In this study, the gel was introduced in an autoclave and the hydrothermal treatment was realized at different temperatures (100 or 120 °C) and with various plateaux (6, 12 or 24 h).

Sol-gel method allows obtaining small $BaTiO_3$ NPs in a soft environment at lower temperatures than with classical co-precipitation method. These small sizes coupled to stabilizing agents coming from precursors might be of interest in the case of biomedical applications. However, reaction time is longer than other methods such as microwave assisted synthesis and scale-up might be an issue because of the difficulty to control reactants' compositions [152].

3.1.3 Hydrothermal and solvothermal synthesis

Hydrothermal synthesis received attention due to the possibility to produce small particles with a well uniform size distribution and a high crystallinity. Prado *et al.* [150] prepared $BaTiO_3$ NPs by various synthesis methods among them hydrothermal and microwave-assisted hydrothermal

syntheses. While particles of approximately 180 nm were formed using conventional hydrothermal synthesis, smaller particles (66 ± 16 nm) were obtained thanks to the microwave-assisted hydrothermal synthesis in lower reaction times (six-fold).

The role of *in situ* stirring under microwave-hydrothermal conditions on the synthesis of $BaTiO_3$ NPs, has been investigated by S. Komarneni *et al.* [15]. Stirring in the temperature range of 150-200 °C enhanced crystallization of $BaTiO_3$ NPs and led to smaller and more uniform NPs compared to those crystallized without stirring (30 nm instead of 60-100 nm). Hydrothermal/solvothermal syntheses include also supercritical fluids approaches. Reverón *et al.* [159] obtained, thanks to a continuous reactor method, $BaTiO_3$ NPs by hydrolyzing isopropoxide precursors in sub and supercritical water/ethanol mixtures (150-380 °C, 16 MPa). The crystallinity of the NPs can be controlled by varying the water/ethanol ratio, achieving up to 90% when the ratio is equal to 1. Mixed oxides can also be produced, for instance $Ba_{0.6}Sr_{0.4}TiO_3$ has been synthesized using the same continuous supercritical chemical processing [158]. The shape of mono-dispersed $BaTiO_3$ NPs has been controlled in a hydrothermal reaction system by Q. Ma *et al.* [157], using oleic acid and tert-butylamine used as surfactant and additive, respectively. The average size of $BaTiO_3$ nanocubes was about 25 nm with a narrow size distribution.

Hydrothermal and solvothermal approaches are more complicated to set-up compared to classical co-precipitation methods. However, once parameters are optimized, such routes are ready for scale-up production and can lead to $BaTiO_3$ NPs obtained without further calcination and with narrow size distribution and good crystallinity. However, due to the preindustrial approach of this method, some impurities such as $BaCO_3$ and/or TiO_2 could be observed after

synthesis [150, 158].

3.1.4 High energy milling

In this approach, two cases must be highlighted: direct mechanosynthesis in the mill and mechanical activation, followed by thermal annealing under softer conditions than classical solid-state reaction. Very few publications report the direct synthesis of $BaTiO_3$ NPs in a mill. Using BaO and TiO_2 as the staring materials, B.D. Stojanovic *et al.* [162] demonstrate that $BaTiO_3$ NPs could be obtained in a planetary ball-mill. The quantity of carbonates was minimized during extended milling time, even if realize under air atmosphere. The resulting perovskite $BaTiO_3$ powder exhibited a particle size in the range of 20-50 nm, rather agglomerated after 240 min of milling. Ohara *et al.* [165] reported the complete formation of $BaTiO_3$ NPs (10 nm) after 12 min of milling, starting from a mixture of $BaCO_3$ (50 nm) and TiO_2 (7 nm) and using an attrition type milling apparatus with a rotating speed of 4000 rpm.

Concerning mechanical activation, wet and dry millings can be considered. In the Sundararajan *et al.* study [161], $BaTiO_3$ NPs were synthesized using high-energy planetary milling approach under wet and dry conditions. Then, the milled powders were calcined at 1000 °C by microwave and conventional heating. Dry milled and microwave calcined $BaTiO_3$ NPs showed the highest value of tetragonality, lowest particle size and highest surface area. In order to improve the kinetics of the solid-state reaction, Ashiri *et al.* [164] milled for 10 h the $BaCO_3$ and TiO_2 starting materials. $BaTiO_3$ NPs (27 nm), free from the secondary phases, were obtained at a lower temperature than classical solid-state reaction (900 °C instead of 1100-1400 °C).

Milling is a common method to obtain $BaTiO_3$ NPs. This approach allows to use lower temperature to obtain crystalline phase, sometimes, by optimization of the milling conditions, the $BaTiO_3$ NPs can be obtained directly in the mill. Classical impurities come from the milling tools. However, as this technique is mainly occurring in dried conditions, NPs produced are agglomerated and hardly redispersible in water and that could be the major issue for biomedical applications [162, 173].

3.1.5 Other approaches

Several other synthesis methods are possible to obtain $BaTiO_3$ NPs for example above the melting point of the chosen salt, the molten salt forms a liquid phase acting as a solvent for reactant dissolution, diffusion and precipitation. $BaTiO_3$ NPs were synthesized by molten salt method using barium hydroxide octahydrate, TiO_2 and the eutectic salts (NaCl-KCl) [160]. NPs can be formed at 600 °C. The crystallinity of $BaTiO_3$ increases with the temperature. Most $BaTiO_3$ NPs display hexagonal shape, with an average size around 50 nm.

Purwanto *et al.* [168] obtained $BaTiO_3$ NPs with tunable size by flame-assisted spray pyrolysis (FASP). Particle size was controlled over a wide range (from about 23 to 71 nm) by varying the concentration of precursor and methane flow rate. Organometallic synthesis uses organometallic precursors dissolved in organic solvents. It provides an ideal environment for controlling $BaTiO_3$ NPs size since the nucleation and the subsequent growth steps are separated. Surfactants or stabilizing agents are usually used in this process for controlling the morphology of the resulting NPs. In a typical procedure, a moisture-sensitive bimetallic alkoxide is injected into mixed solvents of diphenyl ether and oleic acid at 140 °C under inert atmosphere.

Hydrogen peroxide is further injected into the system once it is cooled to 100 °C allowing the hydrolysis of the precursor and the formation of uniform $BaTiO_3$ NPs with a diameter of 8 nm [89]. By the electrochemical synthesis method, Prado *et al.* [150] obtained $BaTiO_3$ NPs with large distribution in particle size (67 ± 20 nm).

Some other approaches lead to bigger structures and morphologies for which the prefix nano if not always appropriate. $BaTiO_3$ tubes have been obtained by templating approach with either a ‘‘hard template’’ (*e.g.* anodic aluminum oxide (AAO) templates or TiO_2) or ‘‘soft template’’ (*e.g.* polymers) [174]. In the Chen *et al.* study [169], the obtained $SrTiO_3$ and $BaTiO_3$ tubes were around 250 nm in diameter and 2.5 mm in length, that is why the term “nano” is not really appropriate for this procedure. Yuh *et al.* [170] obtained $BaTiO_3$ nanofibres *via* electropinning process. After sol/gel synthesis of the $BaTiO_3$ precursor, the solution was mixed with a polymer, here poly(vinyl pyrrolidone) (PVP, Mw=1,300,000) dissolved in ethanol. After being stirred at room temperature for 2 h, the mixture was loaded into a plastic syringe. The electrospun polymer–ceramic composite fibres were heat treated to yield perovskite fibres after annealing at 750 °C for 1 h. Typical fibre diameter was between 80 and 190 nm with fibre lengths exceeding 0.1 mm.

All these other approaches to synthesize $BaTiO_3$ NPs are less common. With molten salt route, particles are obtained with lower calcination’s temperature but their colloidal stability after synthesis might still be an issue. Flame-assisted spray pyrolysis is a one-step method to obtain the desired NPs without further calcination treatment. However, as for milling techniques, the synthesized particles are agglomerated and so not stable in suspension. Electrochemical synthesis has the shortest reaction time but it might be difficult to scale-up such methods as

they'll need high power supply. Template method allows the formation of original and promising shapes but not with nano sizes. It is the same observation for electrospinning approach that leads to interesting nanofibers but not in the nano-range. **Table 1** summarizes the different synthetic process (native and variant form) for $BaTiO_3$ NPs synthesis, highlights their features and summarize their advantages and disadvantages.

Table 1. Summary of different synthetic process (native and variant form) for $BaTiO_3$ NPs synthesis along with their features.

Synthesis	Variant	Phase	Size	Morphology	Advantages/Limits	References
Co-precipitation		Cubic	30-50 nm	Sphere	*Pros* : Simple Well-used *Cons* : Polydispersity Agglomeration if annealing is required Some impurities	[140]
	Sonochemistry + Zr	Cubic	51 ± 6 nm	Sphere		[141]
	Thermal treatment	Cubic/ tetragonal	ND	ND		[142]
	+ Calcination + Ca + Zr	Tetragonal	400-500 nm	Sphere		[143]
	+ Sonochemical	Tetragonal	50 nm	Sphere		[144]
	High-gravity reactive preparation	Cubic	90 nm	Sphere		[145]
	High-gravity reactive preparation	Cubic	60 nm	Sphere		[146]
Sol-gel methods	*+ $Co_{1-x}Ni_xFe_2O_4$ NPs*	Tetragonal	53-95 nm	Quasi-Sphere	*Pros* : Small sizes Low temperature *Cons* :	[147]
	Gel collection	Cubic	8-12 nm	Sphere		[148]
	+ Hydrothermal	Cubic	25 nm	Sphere		[149]
		Cubic	20.5 nm	Heterogeneous		[150]

	+Hydrothermal	Cubic	25-30 nm	Sphere	Long time Scale-up complicated	[171]
	+ Bi doped + calcination	Cubic	32-36 nm	Sphere		[152]
		Cubic	6-12 nm	Sphere		[89]
Hydrothermal	*Under N_2*	Cubic	115 nm	Sphere	*Pros* : Easy to scale-up No calcinaion needed Narrow size distribution Good cristallinity *Cons* : Elaborated set-up Impurities	[146]
		Cubic	44.7 nm	Sphere		[150]
	+ Microwave	Cubic	33.6 nm	Sphere		[150]
	+ Microwave	Cubic	60-100 nm	Sphere		[153]
	+ Stirring	Cubic	30 nm	Sphere		
	+ Hydroxyapatite Nanorods	Cubic	50-100 nm	Nanorod		[154]
	+ Titanate nanotubes	Cubic/tetragonal	50 / 200-500 nm	Helical nanotube		[155]
	+ Eu + 1000 °C	Tetragonal	31-34 nm	Sphere		[156]
	+ Oleic acid	Cubic	25 nm	Cube		[157]
	Supercritical H_2O + Sr	ND	23 nm	Irregular Sphere		[158]
	Supercritical H_2O/EtOH	Cubic	15-36 nm	Irregular Sphere		[159]

Solvothermal		Tetragonal	100 nm	Sphere		[144]
High-energy milling	*Microwave calcination*	Tetragonal	75-80 nm	Sphere	*Pros* : Low temperature Cost effective Scale-up quite easy *Cons* : Agglomerated Large grain size dispersity Hardly dispersible Impurities coming from the grinding tools	[161]
		Cubic/tetragonal	20-50 nm	Sphere		[162]
	Addition of Ag	Tetragonal	800 nm	Sphere		[163]
		Cubic	27 nm	Sphere		[164]
		Cubic	22 nm	ND		[165]
	Microwave calcination	Tetragonal	150 nm	Needle		[166]
	+ Sonication	Tetragonal	64 nm	Heterogeneous		[167]
Other approcahes	*Molten Salt*	Cubic	50 nm	Hexagonal	*Pros* : Low temperature *Cons* : Colloidal stability	[160]
	Pyrolysis	Cubic	23-71 nm	Sphere	*Pros* : One step *Cons* : Agglomerated	[150]
	Electrochemical	Cubic	21 nm	Heterogeneous	*Pros* : Fast *Cons* : Energy consumption	[168]
	Templating	Cubic	250 nm / 2.5 µm	Tube	*Pros* : Original shapes	[169]
	Electrospinning	Tetragonal	Φ 180-360 nm	Fibre	*Cons* : Not “nano”	[170]

3.2 Surface modification of $BaTiO_3$ NPs

All of synthesis methods above-mentioned provide $BaTiO_3$ nanoparticles with unique physical and chemical properties mainly depending on their size and shape. According to recent development of $BaTiO_3$ for biomedical applications, many researcher teams are interested on the surface enhancement method to provide $BaTiO_3$ NPs with appropriate dispersibility and biocompatibility properties. Indeed, $BaTiO_3$ NPs produced by traditional solid-state methods tend to have broad size distributions and poor dispersibility in aqueous media. In this review, we report several surface modification methods such as the hydroxylation, the functionalization with an organic modifier (coupling agent, polymer, zwitterion) or the core-shell formation with an inorganic compound (gold, cobalt ferrite, *etc*). A figure representation of the summary of different functionalization approaches along with their utility for biomedical applications is presented in **Figure 6**.

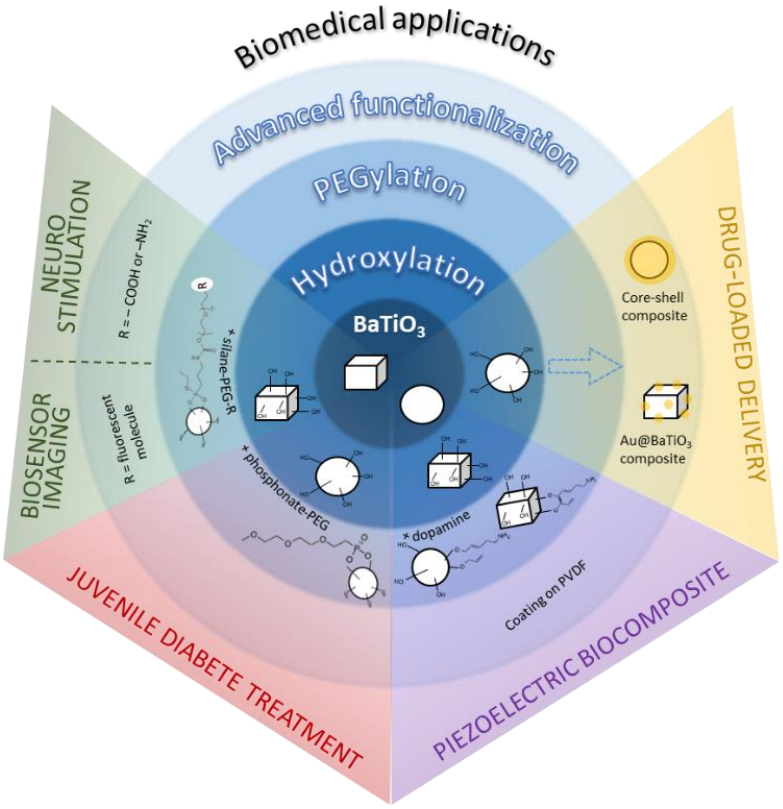

Figure 6. Schematic representation of different functionalization approaches for numerous biomedical applications of $BaTiO_3$ NPs.

3.2.1 Hydroxylation

$BaTiO_3$ NPs have high surface energy and large surface area which tend to form large aggregates when there are dispersed in aqueous media [111, 175]. Hence these next decades, the hydroxylation of pristine $BaTiO_3$ surface became a common surface activation method before any surface modification such as functional ligand or core-shell formation with metallic element [81, 83, 176-178].

Generally, the hydroxylation of $BaTiO_3$ NPs surface is occurred *via* a thermal decomposition

of hydrogen peroxide (H_2O_2). Refluxing H_2O_2 at high temperature (106 °C) in an aqueous solution containing the nanoparticles derives the free hydroxyl groups [179, 180]. However, this heating temperature is closed to the Tc where the material undergoes a transition between its ferroelectric and non-ferroelectric structures [63]. Hydroxylating NPs at high temperature could damage piezoelectric properties and hinder their potential for theranostic applications. Jordan *et al.* conducted a study about hydroxylating at 85 °C while varying the reaction time from 30 min to 8 h [83]. By a FTIR investigation of the O-H bond stretching located at 3900-2800 cm^{-1} and according to a statistical study, they showed that the longer is the reaction time the higher is the magnitude peak. The OH level coverage quantification was performed by a spectrofluorometer after the grafting of a bifunctionalized polyethylene glycol (PEG) with a fluorescent moiety. For the sample after a hydroxylating during 8 h, 15 ± 1.5 fluorescent PEGs were counted while 6.9 ± 0.55 were counted for 1.5 hours reaction time and only 5.6 ± 1.5 for an unmodified $BaTiO_3$ NPs. This result means that higher is the reaction time, denser is the hydroxyl coverage which will provide more available binding reactive sites for surface modification. After washing and drying, the modified $BaTiO_3$ is able to be used for surface modification without any other treatments.

3.2.2 Modification with an organic modifier

In addition to the different sizes and shapes obtained after synthesis methods, surface composition of $BaTiO_3$ NPs is considered to be one of the key factors that affect their chemical/colloidal stability and biocompatibility. An improvement of the stability has been observed by covalently attaching organic monolayers onto oxides [181, 182]. The most common approach to both stabilization and functionalization/targeting of the metal oxides nanoparticles

is the grafting of PEG molecules, also named "pegylation" [183-185]. PEG has no affinity to metal oxide surface and need to have special active moieties to be introduced to ensure the grafting [186]. These special moieties could be for example silane or phosphonate [41, 187-189]. Generally, the used PEG is heterobifunctional and the second end of the polymer chain is the targeting biomolecules for imaging or therapeutic applications.

3.2.2.1 Silane

Surface modification with a silane-PEG is similar to the one with alkoxysilane coupling agent which is one of the most commonly used methods to prepare monolayers on oxides including $BaTiO_3$ [190, 191]. The main advantage of using silanes for monolayer formation on oxidic surfaces is the rapid formation of a covalent bond between the OH surface onto the substrate and the anchoring group. The general silanization process is a solution-phase reaction between the hydroxyls on the surface of BTO and the silane agent following a three-step mechanism. Firstly, the initial hydrolysis of alkoxysilanes occurs where trialkoxy groups turned into trihydroxyl groups. Then, the trihydroxyls groups react with the ones on the oxide surface and form hydrogen bonds followed by a condensation to create covalent bonds [192].

The recent results of Jordan *et al.* are a good example of the large pegylation capacity of $BaTiO_3$ in order to be used in many theranostic applications such as cancer imaging, brain stimulation or therapy [83]. They developed methods to tune the $BaTiO_3$ fluorescence properties to be able to work with standard 488 nm, 532 nm and 633 nm fluorescent light sources. Indeed, green fluorescent PEG is readily available but for many applications it is require another fluorescent spectrum. By coating modified PEG obtained by mixing silane-PEG-SH with sulfocyanine3

maleimide or silane-PEG-NH_2 with suflocyanine5 NHS ester, orange and red fluorescent $BaTiO_3$ NPs were obtained, respectively. Furthermore, the authors highlighted the impact of the pegylation on the surface charge and found a way to tune it according to the desired applications. For example, a positively charged polymers enhanced the interactions with cells membranes and increased cellular uptake [41] Depending on the nature of the second function of a silane-PEG, the ζ-potential can be tuned either more negatively if it is a carboxylic moiety or more positively if it is an amine moiety. The reaction with a silane-PEG-SH provided an antibody conjugation potential of $BaTiO_3$ NPs. The study on the specific monoclonal anti-EGFR antibody (225) and a human epidermoid carcinoma cells (A431 cell line) concluded on the $BaTiO_3$-PEG-SH efficiency for molecular targeting.

3.2.2.2 Phosphonate

Pazik *et al.* worked on the functionalization of $BaTiO_3$ NPs with phosphonate molecules by pegylation to provide biocompatible coating properties for an application in the treatment of juvenile diabetes [188]. The studied phosphonate-based modifiers were ethylphosphonic acid (EPA), aminoethylphosphonic acid (AEPA), imino-dimethylphosphonic acid (IMPA), nitrile-trimethylphosphonic acid (NMPA), adenosine-5'-triphosphate (ATP), phosphocreatine (PCr) and γ amino-butyric acid (GABA). Results in ^{31}P NMR confirmed the strong interaction between modifying agents and oxide surface and concluded on a successfully covalent and stable surface modification for all grafted molecules. DLS and ζ-potential analysis showed that the most stable suspensions of $BaTiO_3$ NPs (with an average diameter of 5 nm) were produced with ATP modifier. The hydrodynamic size with ATP was to be only 101 nm while the value is more than 300 nm for the others phosphonate coupling agents. The ζ-potential was equal to

-35.1 mV for ATP modifier whereas it was closer than -25 mV for the others molecules. In sum, the charge and the steric stabilization showed clearly a better dispersion of the ATP-modified particles.

3.2.2.3 Dopamine

The elaboration of biocomposite based of the mix of $BaTiO_3$ and PVDF is a new effective approach to synergize the advantages of both organic and piezoelectric materials [193]. However, the poor interfacial adhesion between the rigid piezoelectric material and flexible polymers enable a direct coupling. To address this concern, surface modification of the oxide particles *via* dopamine (DOPA) was employed as a linker. Su *et al.* developed a method where dopamine encapsulated $BaTiO_3$ NPs after reaction with the oxide surface hydroxyl groups. Then, a high electric field during electrospinning was applied which allows positively charge amine group to form stable hydrogen bonds with the difluoromethylene groups of PVDF chain. The successful deposition of PDA-modifier layer was defined by SEM analysis where a uniform thickness of amorphous material was observed around the surface of each oxide nanoparticles [194].

3.2.3 Modification with an inorganic compound

$BaTiO_3$ nanoparticles can also be coupled with metallic elements like gold or with a semiconductor like TiO_2 in order to modulate the electrical properties thanks to its specific piezoelectric ability.

3.2.3.1 Gold nanoparticles

With their specific plasmonic properties, gold nanoparticles (AuNPs) are widely used in cancer treatment by noninvasive method like photothermal therapy. The linkage of AuNPs with $BaTiO_3$ could follow either a core-shell method [195, 196] or a deposition-precipitation method [197]. Wang *et al.* synthesized a $BaTiO_3$-core Au-shell composite by Duff and Baiker method after a preliminary amino-functionalization of the oxide surface. Briefly, $BaTiO_3$ was firstly treated with H_2O_2 to activate the surface. Then, NPs were functionalized with an amino-function before being mixed with a gold colloidal suspension to form $BaTiO_3$ NPs seeds. $BaTiO_3$ NPs seeds are allowed by an overnight reaction between small Au colloids (2-3 nm) and aminated- $BaTiO_3$ NPs. Then, the full gold shell is reached after that $BaTiO_3$ NPs seeds have been reacted with a gold chloride solution ($HAuCl_4$) in presence of formaldehyde. This method leads them to a nanoparticles size with an average hydrodynamic diameter around 83 nm composed with an Au shell thickness ~10 nm and a core diameter of ~80 nm. Their applied study showed that irradiation of tumors in animals with the injected intravenously nanocomposite lead to an efficient photothermal effect at irradiances that did not result in thermal injury [195].

Wu *et al.* synthesized an Au@$BaTiO_3$ composite based on the growing of AuNPs on the $BaTiO_3$ surface by deposition-precipitation method. Typically, they previously synthesized $BaTiO_3$ NPs by hydrothermal method and dispersed the obtained-nanocubes in a gold salt solution to obtain oxide nanocubes decorated by gold nanoparticles (size diameter ≈ 3 nm) [28]. Their recent results showed that the as-created Schottky junction and the piezoelectric effect allow the nanocomposite to be used as a novel sonosensitizers for bacterial killing and wound repair [197].

3.2.3.2 Others

Shahzad *et al.* spotlighted the interest to develop another core-shell nanocomposite based on $CoFe_2O_4$@$BaTiO_3$ for targeting cancer therapy. The main problem to obtain a such nanocomposite is related to the agglomeration effect. Indeed, to exploit the advantage of the combination of a magnetic core surrounded by a piezoelectric shell, each $CoFe_2O_4$ magnetic core should be completely wrapped by a piezoelectric $BaTiO_3$ shell. This includes good dispersibility because unwrapped parts due to agglomeration could cause leakage current and disturb the required magnetoelectric properties during cellular interactions. For that reason, a synthesized method by sonication was used and a core-shell morphology with a 26 nm diameter size for the core and around 6 nm diameter for the shell was obtained. The potential efficiency in nano carrier's application was carried out with two drugs: doxorubicin (DOX) and methotrexate (MTX). The drugs loaded onto nanocomposites were obtained after a polymer coating which provide free carboxylic acid groups on the particles surface to react with an amine groups *via* EDC (1-(3-Dimethylaminopropyl)-3-ethylcarbodiimide hydrochloride) chemistry. For both drugs, results indicated that magnetoelectric $CoFe_2O_4$@$BaTiO_3$ nanocomposite is effective as drug carrier and show promising future for cancer therapy under external magnetic-field [198]. **Table 2** summarizes the different strategies of surface modification and highlight their advantages.

Table 2. Summary of different strategies of surface modification for $BaTiO_3$ NPs in biomedical application

Stratégies of surface modification	**Modifier agents**	**Advantages**	**Ref.**
Hydroxylation	H_2O_2	Improve the surface activation of $BaTiO_3$ nanoparticles	[179, 180]
Organic modifier by pegylation	Mix of silane-PEG-SH with sulfocyanine3 maleimide / Mix of silane-PEG-NH_2 with sulfocynanine5 NHS ester	Rapid formation of a covalent bond between OH surface onto the substrate and the anchoring group	[83]
Organic modifier by pegylation	Silane-PEG-COOH and silane-PEG-NH_2	Possibility to tune the surface charge	[41]
Organic modifier with based-phosphonate molecules	Ethylphosphonic acid (EPA), aminoethylphosphonic acid (AEPA), imino-dimethylphosphonic acid (IMPA), nitrile-trimethylphosphonic acid (NMPA), adenosine-5'-triphosphate (ATP), phosphocreatine (PCr) and γ amino-butyric acid (GABA)	Provide biocompatible properties with a control of the charge and steric stabilization	[188]
Organic modifier	Dopamine	Dopamine acts like a bridge to pre-functionalize $BaTiO_3$ to be then coupling with polyvinylidene fluoride (PVDF)	[194]
Core-shell modification	Gold nanoparticles	Modulation of the electrical properties, lead to an efficient photothermal effect in cancer therapy application	[195, 196]
Metalic nanoparticles surface modification	Gold nanoparticles deposit onto the oxide surface by deposition-precipitation method	Provide new electrical properties and lead to a novel sonosensitizers for bacterial killing and wound repair	[197]
Core-shell modification	$CoFe_2O_4$	New electrical properties and lead to effective NPs for drug carrier in cancer therapy	[198]

4. $BaTiO_3$ NPs-based nanocomposites and their applications

4.1 Drug/gene delivery, cancer therapy, and bioimaging

Due to excellent biocompatibility and unusual nonlinear optical characteristics, $BaTiO_3$ NPs has been used as nanocarriers or piezoelectric layer in actuators for drug delivery applications and as label-free imaging probes [38, 199]. $BaTiO_3$ NPs exhibited the optimal cytocompatible behavior even at higher amount (100 μg/ml) and enhanced the efficiency of doxorubicin (DOX; a chemotherapy drug) upon supramolecular complexation [200]. Further, electric potential can be produced by $BaTiO_3$ NPs in remote modality using ultrasound effect, wherein mechanical pressure waves are safely and effectively carried to deep tissues. As the utmost usual and detrimental primary brain tumor among adults in categorized by glioblastoma multiforme (GBM), the leading difficulties in treating GBM are related to the attained resistance to chemotherapeutic drugs and recurrence of cancer after surgery in connection to residual tumor micro-foci.

Multidrug resistance of chemotherapeutic molecules often results due to overexpression of membrane glycoproteins known as P-glycoprotein (P-gp) encoded by MDR1 gene, which lacks substrate specificity due to recognition of diverse chemical structures leading to wide spread substrate specificity and cross-resistance [201]. To address this issue, electric simulation of piezoelectric materials has reported to be an interesting approach to alter biological activities of biological cells [202, 203]. In this case, low-intensity electric stimulation acts for reducing multidrug resistance of cancer/tumor (without affecting healthy cells). Here, specific MDR1 inhibitors such us Tariquidar (XR9576) are stimulated while inducing significant anti-

proliferative consequences by affecting Ca^{2+} and K^{+} homeostasis and by obstructing the arrangement of mitotic spindles. Therefore, Marino *et al.* developed ultrasound-responsive piezoelectric NPs to deliver electric stimulations remotely to glioblastoma cells. [204]. Herein, $BaTiO_3$ NPs were modified with an antibody against the transferrin receptor (TfR) (abBTNPs) for getting dual action by furnishing potential to cross the blood-brain barrier (BBB) and targeting glioblastoma cells through *in vitro* 2D transwell model utilizing cultures of immortalized brain-derived endothelioma bEnd.3 cells and glioblastoma cell line (U-87 cells). In this configuration, endothelial layer separates the top compartment (luminal) from the bottom compartment (abluminal). These ultrasound-responsive piezoelectric NPs remarkably decreased the proliferation of glioblastoma cells *in vitro* and enhanced the sensitivity to chemotherapeutical action with significant anti-proliferative and pro-apoptotic outcomes **(Figure 7)**.

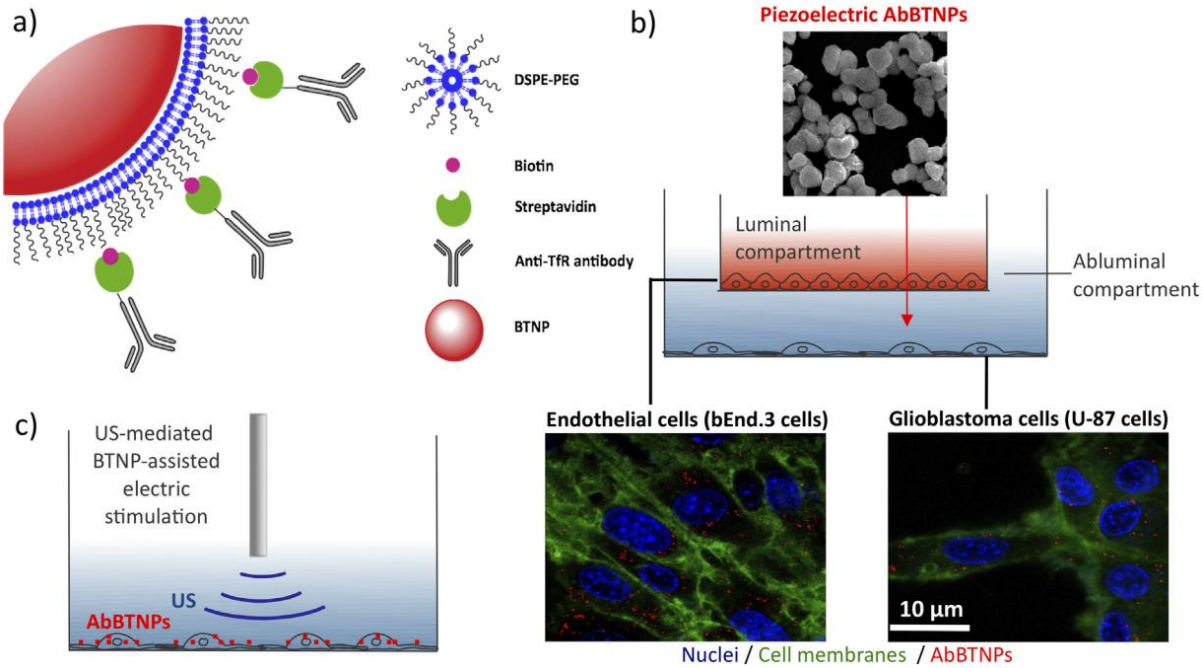

Figure 7. (a) Functionalization of $BaTiO_3$ NPs with antibody against TfR, (b) NPs crossing *via* a static 2D model of the BBB (nuclei, cell membranes, and $AbBaTiO_3$ NPs are shown in blue, green and red color, respectively), and (c) chronic ultrasonic-sensitized piezoelectric-stimulation of glioblastoma cells. Reproduced with permission. [204] Copyright 2019, Elsevier.

In another study, the surface of $BaTiO_3$ NPs has been modified by hydroxylation, then coated with the hydrophilic poly (ethyl glycol) (PEG). In addition, the conjugation of anti-EGFR antibodies to the surface of $BaTiO_3$ NPs exhibited effective molecular targeting of NPs to epithelial cells (A431 cells). The surfaced-functionalized $BaTiO_3$ NPs expand the applications possibly in cancer therapy, molecular imaging, or non-invasive neurostimulation [83].

Further, a core-shell structure of $BaTiO_3$ nanospheres (as core) and gold (Au; as nanoshells) has been synthesized, wherein core nanospheres were functionalized by (3-aminopropyl) triethoxyysilane (APTES) having exposed surface amine groups. The core-shell structure showed the shifting of surface plasmon resonance (SPR) position of nanoshells from visible to near infrared (NIR) region of electromagnetic wave, having potential biological interest [205] with potential to be utilized in bioimaging areas. However, $BaTiO_3$ NPs exhibit low level of cellular uptake efficacy, which was improved by coating of the NPs using polyethylenimine (PEI, a cationic polymer and one of the most effective nonviral gene delivery agents). The PEI coated $BaTiO_3$ NPs demonstrated 8-fold enhancement in cellular uptake capacity and achieved high amounts of gene delivery with the complex of PEI@$BaTiO_3$/DNA (nucleic acids). The complexed platform showed great potential in coupled imaging and gene therapy [41].

To explore the magnetoelectric influence $BaTiO_3$ based nanocomposites in a study, various

core-shell types magnetoelectric NPs ($CoFe_2O_4$-$BaTiO_3$, $CoFe_2O_4$-$Bi_4Ti_3O_{12}$ and Fe_3O_4-$BaTiO_3$) have been synthesized and modified with poly (N-isopropylacrylamide) (PNIPAM). The obtained thermo/magnetic-sensitive nanocarriers were evaluated for the adsorption and release kinetics of methotrexate drug by using mathematical modelling. All NPs exhibited similar physicochemical behavior (e.g., drug release patterns) and are responsive to both temperature and alternative magnetic fields, however overall drug release was attained only under magnetic effects. Furthermore, methotrexate interparticle-confined led in an incomplete release at temperatures below or above the lowest critical solution temperature of PNIPAM [206]. In another study, core-shell magnetoelectric cobalt ferrite@$BaTiO_3$ nanocarriers with colloidal stability have been synthesized and conjugated with anticancer drugs (DOX and methotrexate) with up to 80% functionalization via EDC chemistry. Under external magnetic field of 5 mT, magnetoelectric nanocarriers showed significant improved cytotoxicity to human hepatocellular carcinoma (HepG2) and human malignant melanoma (HT144) as compared to drug-free or without field repetitions [198]. Furthermore, tumor-treating fields (TTF) supply alternating electric fields of low intensity (1-3 V/cm) and intermediate frequency (100-300 kHz) *via* non-invasive transducer arrangements within the anatomical area of tumor [207, 208]. On considering it, the effect of TTF-responsive sensitizer ($BaTiO_3$ NPs) has been demonstrated on breast cancer cells (BCCs), wherein they sensitize TTF-resistant BCCs and $BaTiO_3$ NPs accumulated in the cytoplasm of BCCs in response to TTF. Moreover, TTF-responsive $BaTiO_3$ NPs showed antitumor action by controlling various breast cancer-related routes, particularly cell cycle-related apoptosis route [209]. The anticancer effect of $BaTiO_3$ NPs was also studied in breast cancer cell line, MCF-7 with almost 57% reduction in cell viability was observed for a

maximum concentration of 200 µg/mL of $BaTiO_3$ NPs [210]. In another study, core-shell magnetoelectric nanoparticles of $Co_{0·8}Mn_{0.2}R_{0.02}Fe_{1·98}O_4$ (CoMnRFe) (R = Ce, Eu, Tb, Tm, or Gd) (core) and $BaTiO_3$ NPs (shell) was prepared by Alfareed *et al.* to study the anticancer activity of the designed system on human colon cancer cells (HCT-116) [211]. The toxicity assessment of these core-shell nanoparticles was also analyzed in HEK-293 cells to emphasize minimal toxic effect of these nanoparticles on normal cells.

The size and morphology of $BaTiO_3$ NPs are important factors that could decide its pattern and efficiency of cellular internalization. However, other attributes like dielectric properties and piezoelectric effect could also be vital in its assessment as an effective drug/gene delivery system. The burst release of the drug from the nanocarriers is a major issue in local drug delivery applications. Therefore, a dam-like property due to piezoelectric activity was introduced on TiO_2 nanotubes by the coating of $BaTiO_3$ to prepare TiO_2@$BaTiO_3$ co-axial nanotubes. Herein, the free diffusion rate of the drug (vancomycin hydrochloride; VMH) loaded onto TiO_2@$BaTiO_3$ co-axial nanotubes was decreased by dam-like action and the cumulative release of high VMH concentration was decreased by 54.8% when evaluated for 7 days. Also, the polarized VMH/TiO_2@$BaTiO_3$ co-axial nanotubes showed long-term antibacterial efficacy on Staphylococcus aureus [212]. The association of $BaTiO_3$ could be useful in providing additional features like sustained release of drugs, antimicrobial properties to the already existing delivery systems, marking its utility as a potent carrier platform.

Osteosarcoma (OS) is a hostile malignant neoplasm, which arises from embryonic transformed cells of mesenchymal origin and encourage osteoblastic differentiation and create malignant

osteoids [213, 214]. The clinical treatments such as surgery or high-dose chemotherapy are promising and effective in treating OS, but various side effects, including second malignancies and tumor metastasis [215, 216] have been observed with increased drug resistance [217]. In this regard, hyperthermia has been considered as an effective adjuvant therapy for carcinoma and sarcomas after surgical treatments [218, 219]. On considering it, Sasikala *et al.* developed piezomagnetic nanoparticles (PMNPs) composed of $BaTiO_3$ and superparamagnetic iron oxide (Fe_3O_4) for the multimodal anticancer therapy, imaging, and non-invasive cell stimulation. Here, the ferroelectric core of PMPNs is composed of the piezoelectric $BaTiO_3$ NPs surrounded by ferromagnetic shell of superparamagnetic iron oxide nanoparticles to offer excellent electromagnetic properties. The efficacy of the fabricated PMNPs was evaluated for post-surgical osteosarcoma healing, diagnosis, and bone regeneration (collectively termed as Theranogeneration). These PMNPs showed remarkable anticancer activities to eliminate the residual osteosarcoma cells by using magnetic hyperthermia. Further, the study also reported the strong absorbance at 808 nm (due to transition from Fe^{2+} - Fe^{3+} valance states along with the intrinsic absorption properties of $BaTiO_3$ NPs) with concentration dependent intensity increment designating their utility as a potential photothermal agent for photothermal therapy. $BaTiO_3$ NPs have also been reported to generate ROS which can further be explored for their utility in photodynamic therapy for cancer treatment. In addition, the imaging proficiency of PNMPs was also evaluated as a contrast agent for computed tomography. The conjugation of risedronate R (RIS) as bisphosphonate drug to PMNPs instructed bone getting characteristic to PMNPs. Therefore, under low-intensity pulsed ultrasound (LIPUS) and LIPUS-facilitated RIS release from PMNPs demonstrated the improved bone regeneration and thereby helped in

repairing large bone defects caused by osteosarcoma resection [220] **(Figure 8)**.

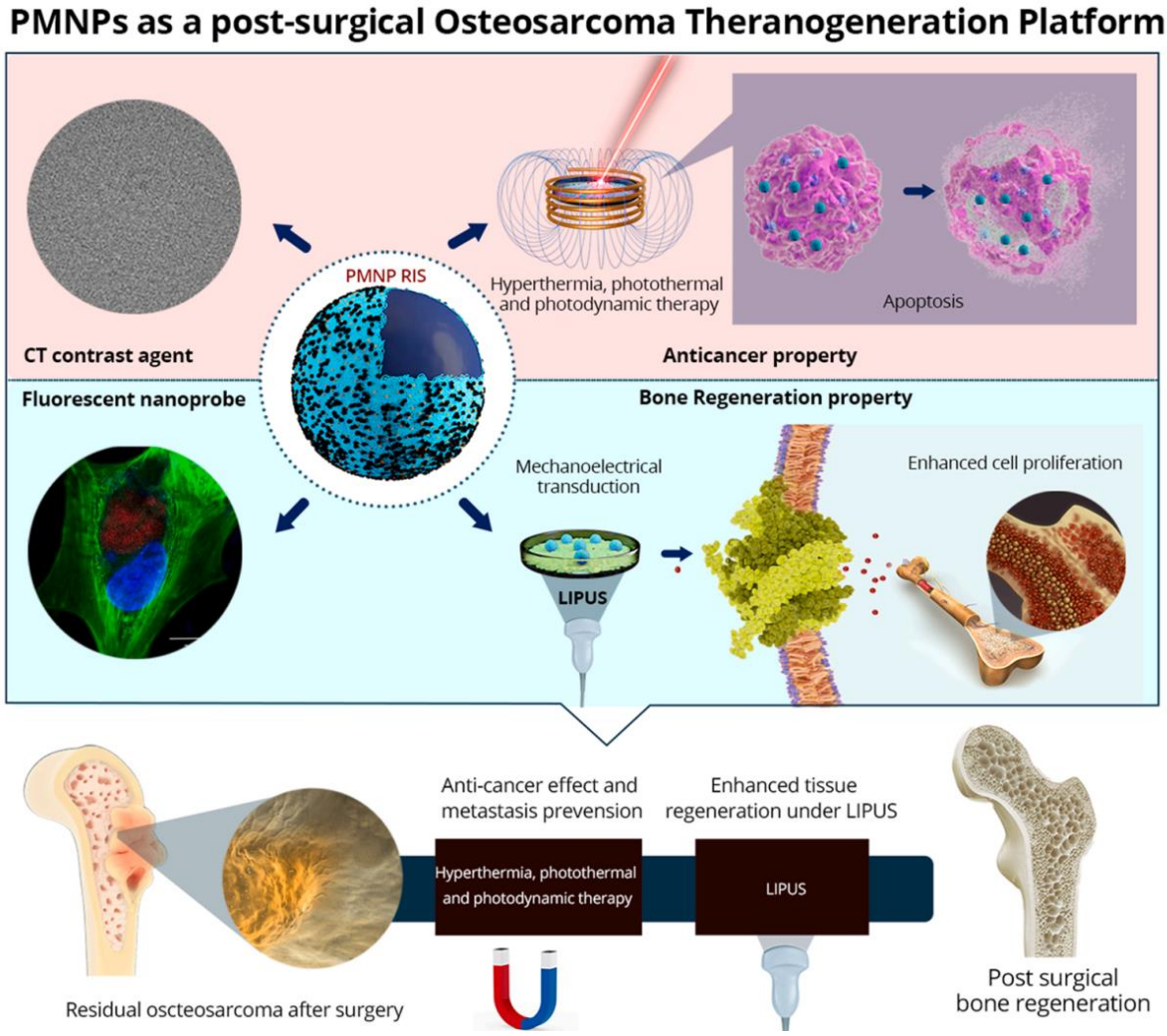

Figure 8. Schematic representation of the phase-wise treatment efficacy of PMNPs for the eradication of osteosarcoma, leading to subsequent osteogenesis. Reproduced with permission. [220] Copyright 2022, Elsevier.

The use of heating effect (*i.e.* hyperthermia) has been promising approach to treat cancerous lesions. Herein, photothermal treatment is considered as a non-invasive and selective healing of cancer. On considering this therapy, $BaTiO_3$ (core)-Au (shell) NPs for hyperthermia healing

against cancer cells have been synthesized. Here, the gold shell was coated on the surface of $BaTiO_3$ NPs via seed mediated growth mechanism where the negatively charged gold nanoparticles were initially electrostatically attached to the positively charged APTES functionalized $BaTiO_3$ NPs. No remarkable variations in cell viability were detected up to 50 µg/ml of NPs and exhibited the ability to destroy human neuroblastoma cells under NIR laser light [196]. The study emphasized on the bioelectric interface of using this fabricated core-shell nanoparticle for future applications.

In another study, sub-100 nm core-shell $BaTiO_3$/Au NPs with bimodal imaging proficiencies have been developed and demonstrated the photothermal consequences, wherein $BaTiO_3$/Au NPs showed efficient absorption of NIR light and converted into heat to remove tumors. Further, the intrinsic dual imaging ability (*i.e.* core $BaTiO_3$ imaged by second harmonic generation and Au shell produces two-photon luminescence) permitted the distribution of NPs in tumor vasculature morphology during photothermal eradication. This study facilitated the *in vivo* real-time tracking of $BaTiO_3$/Au NPs and thermal-induced consequence on tumor vessels [195]. All these studies reflect the association of $BaTiO_3$ with imaging contrast agents have proved its worth as a multifaced candidate for theranostics applications.

The influence of $BaTiO_3$ NPs in both native form and composites on the cell viability, mitochondrial membrane, cellular internalization, and cell division are principal factors that regulates the transportation of biomolecules across tumor tissues. The capacity of $BaTiO_3$ NPs based delivery system to encapsulate the biomolecules and further their release behavior is influenced by the surrounding microenvironment. $BaTiO_3$ NPs based drug delivery systems has opened a new platform in cancer therapy and deserves in depth investigation and

understanding. **Table 3** summarizes the different compositions of $BaTiO_3$ NPs along with their functionalization strategies used in cancer treatment.

Table 2. Summary of different compositions and functionalization strategies of $BaTiO_3$ NPs used in cancer treatment.

Composition	**Functionalization**	**Application**	**Cell line**	**Ref.**
PEG coated $BaTiO_3$ NPs	Antibody	Cancer therapy	Human epidermoid carcinoma (A431)	[83]
$BaTiO_3$ @Gold core-shell nanoparticles.	Thiolated PEG	Photothermal therapy, Bimodal Imaging	Primary Human Umbilical Vein Endothelial (HUVAC) cells	[195]
$BaTiO_3$ NPs@Gold core-shell nanoparticles.	NA	Hyperthermia	Human neuroblastoma (SH-SY5Y) cells	[196]
$CoFe_2O_4$@$BaTiO_3$ core-shell nanoparticles.	Doxorubicin, Methotrexate	Drug delivery	Hepatocellular carcinoma (HepG2) cells, Malignant human melanoma (HT144) cells	[198]
1,2-distearoyl-sn-glycero-3-phosphoethanolamine-N-[methoxy(polyethylene glycol)-5000] coated BaTiO3 NPs	Anti-transferrin receptor antibody	Multimodal imaging, Ultrasound stimulations, Drug delivery	Human primary glioblastoma (U-87) cells	[204]
1 $CoFe_2O_4$@$BaTiO_3$, $CoFe_2O_4$@$Bi_4Ti_3O_{12}$ and Fe_3O_4@$BaTiO_3$ core-shell nanoparticles	PNIPAm	Drug delivery	NA	[206]

Fetal bovine serum (FBS) coated $BaTiO_3$ NPs	NA	Sensitizing antitumor action of Tumour Treating Fields	Breast cancer (MCF-7), (BT-549), and (MDA-MB-231) cells	[209]
$BaTiO_3$ NPs	NA	Cancer therapy	Breast cancer (MCF-7) cells	[210]
$Co_{0·8}Mn_{0.2}R_{0.02}Fe_{1·98}O_4$ (CoMnRFe) (R = Ce, Eu, Tb, Tm, or Gd) @ $BaTiO_3$ NPs		Cancer therapy	Human colon cancer (HCT-116) cells, Non-cancerous (HEK-293) cells	[211]

4.2 Tissue engineering and wound healing

Tissue engineering is a promising approach to repair or regenerate damaged tissues that encounters wear and tear in day-to-day life. Different biomaterials, including polymers (natural or synthetic), nanomaterials (organic or inorganic) or their combination play an important role in designing biomaterial scaffolds for tissue regeneration. Under optimal conditions, suitable biomaterial scaffold with growth factors and signaling molecules enables the adhesion, proliferation, migration, and differentiation of cells for helping in restoring damages tissues [221-224]. In this regard, perovskite ceramic NPs has been utilized to develop scaffolds for mimicking the chemical, mechanical, electrical, and biological characteristics similar to natural tissues [225-228] and shown a great potential in developing composite scaffolds for various tissue engineering, especially hard tissue regeneration [229, 230]. Among other perovskite ceramics, $BaTiO_3$ NPs are more promising in developing tissue engineering scaffolds due to their excellent biocompatibility and peculiar non-linear optical characteristics that can be used to

improve the performance in microscopy for tissue imaging [38, 231] as well as electrical characteristic with high piezoelectric coefficient [232]. Theses facets have made $BaTiO_3$ NPs as a compelling contender for tissue engineering/wound healing applications.

Sonodynamic healing has been believed to be a minimally invasive treatment for eliminating pathogen and curing cancer with high spatial and temporal precision. Therefore, a novel sonosensitizer (Au@$BaTiO_3$) has been developed for highly efficient sonodymanic healing. The study evaluated the generation of reactive oxygen species (ROS) under the influence of ultrasonic waves, thereby establishing the utility of the fabricated nanoparticles as an effective sonosensitizer for sonodynamic therapy for antibacterial attributes. Furthermore, *in vitro* and *in vivo* studies demonstrated that the sonodymanic effect also accelerated the migration of fibroblasts, contributing to the healing of dermal wound in mice [197]. In another study, the surface of TiO_2 nanotubes was modified with $BaTiO_3$ NPs by preserving nanotube structure (TiO_2@$BaTiO_3$ co-axial nanotube) and utilized for coating the surface of titanium alloy with the piezoelectric properties for an effective drug delivery and bone repair [233]. Titanium scaffolds are advantageous for large bone defects, but they are lacking the electrical activity and limit their full utilization in bone regeneration [234, 235]. Therefore, the surface of porous titanium scaffold (Ti-6Al-4V) has been modified with $BaTiO_3$ ceramic and evaluated for *in vitro* and *in vivo* studies under LIPUS. The activity of bone marrow mesenchymal stem cells was remarkably higher in $BaTiO_3$-coated Ti-6Al-4V+LIPUS, $BaTiO_3$-coated Ti6Al4V, Ti-6Al-4V+LIPUS scaffolds than that of Ti-6Al-4V scaffold. Also, a significant improvement in osteogenesis and osteointegration in treated scaffolds, specifically $BaTiO_3$-coated Ti-6Al-4V+LIPUS, was observed after implantation for 6 and 12 weeks in large segmental bone

defects (radius rabbits) as compared to Ti-6Al-4V scaffold [235].

Although, $BaTiO_3$ NPs provides a platform to display piezoelectric activity, its application in tissue engineering is limited owing to its poor bioactivity and osteoconductivity. Since natural bone has piezoelectric character, $BaTiO_3$ owing to its high piezoelectricity has been considered effective in accelerating bone regeneration. Inspired by this, Ahmadi *et al.* demonstrated that the incorporation of Ca^{2+} ions into $BaTiO_3$ NPs ((Ba_xCa_{1-x}) TiO_3) not only decreased the dielectric constant of the system, but also improved the bioactivity and showed remarkable increase in the proliferation of MG63 cells [236]. As said just before, $BaTiO_3$ lacks of bioactive ions that are useful in contributing to osteogenesis. In this regard, calcium ions (Ca^{2+}; plentiful in bone mineral) and manganese ions (Mn^{4+}; key doping element for HAp) were separately or co-doped into $BaTiO_3$ nanofibres through sol-gel/electrospinning/calcination process. The ion-doped $BaTiO_3$ nanofibres exhibited piezoelectric coefficient (d_{33}) of 0.9-3.7 pC/N comparable to natural bone tissue (0.7-2.3 pC/N). Synergistically, Mn^{4+} (2 mol%) and Ca^{2+} (10 mol%) co-doped $BaTiO_3$ nanofibres showed highest ability in improving osteogenic differentiation of bone marrow MSCs without any cytotoxicity [237]. Similarly, in another study, the strontium (Sr) was introduced into $BaTiO_3$ NPs (($Ba_{0.7}Sr_{0.3}$)TiO_3) and then utilized in 3D printing of (($Ba_{0.7}Sr_{0.3}$) TiO_3)/β-tricalcium phosphate (β-TCP) based bioactive and piezoelectric bone scaffolds. The (($Ba_{0.7}Sr_{0.3}$) TiO_3)/β-TCP scaffolds with 60% (($Ba_{0.7}Sr_{0.3}$)TiO_3) and 40% β-TCP exhibited highest mechanical performances (compressive strength, bending module, elastic and young's modulus), however the dielectric constant was improved further with the incorporation of ($Ba_{0.7}Sr_{0.3}$)TiO_3 content in the 3D printed construct. Also, (($Ba_{0.7}Sr_{0.3}$)TiO_3) 60%/β-TCP40% scaffold exhibited highest *in vitro* biomineralization activity (bone-like apatite deposition) after

28 days of incubation in simulated body fluid (SBF) as well as the higher activity of osteosarcoma cells as compared to other composites [238]. In another study, the effect of ((Ba_xZr_{1-x}) TiO_3) was investigated on the properties of β-TCP composite scaffolds, which have been fabricated by using solid-state reaction process. The results showed improvement in electrical properties (e.g., dielectric, ferroelectric, and piezoelectric activities) and mechanical properties (*i.e.* hardness) with the incorporation of $(Ba_xZr_{1-x})TiO_3$ NPs, whereas apatite-forming ability was reduced [239]. Furthermore, calcium silicate (CaS) (akermanite, $Ca_2MgSi_2O_7$) has been utilized with $BaTiO_3$ to prepare porous bioactive scaffold with satisfactory piezoelectric coefficient (d_{33}) and compressive mechanical properties with no cytotoxic behavior with human bone marrow MSCs [240]. In a study, calcium phosphate (CaP) and $BaTiO_3$ NPs have been deposited on bacterial cellulose (BC) membranes using ultrasonic irradiation effect followed by a thermal treatment (1000 or 1200 ^oC) to remove polymeric template to achieve 3D porous structures. The obtained CaP/$BaTiO_3$ scaffolds exhibited cytocompatibility behavior with mesenchymal stem cells (MSCs) [241]. The properties and morphology of $BaTiO_3$ NPs are not severely affected by change in the processing conditions and can withstand high temperature, pressure and irradiation. This is very important aspect marking the versatility of $BaTiO_3$ NPs in numerous applications.

The combination of hydroxyapatite (HAp) and $BaTiO_3$ NPs have shown a great potential in fabricating biocompatible, mechanical improved and electro-active prosthetic orthopedic graft material [242-244]. In two separate studies, aligned porous piezoelectric scaffolds composed of HAp and $BaTiO_3$ NPs showed the remarkable compressive strengths (~14.5 MPa and ~34.7), porosities (~57.4% and ~50%), and piezoelectric coefficient d_{33} of 2.8 pC/N and 5.0 pC/N

(greater than that of natural bone tissue) and demonstrated no cytotoxicity to the fibroblasts (L929 cells) as well as accelerated attachment, proliferation, and differentiation of MG63 cells [245, 246]. Similarly, hydroxyapatite (HAp)/$BaTiO_3$ and α-TCP/$BaTiO_3$ composite scaffolds have been fabricated and sintered (500-1300 ^oC) under various atmospheres. The higher phase stability was observed in α-TCP/$BaTiO_3$ scaffold compared to HAp/$BaTiO_3$ scaffold. In HAp/$BaTiO_3$ scaffold, by-product phases of $CaTiO_3$ and Ba_2TiO_4 were formed at around 900 ^oC, whereas these by-products associated with the low concentration of $BaTiO_3$ NPs were detected at sintering temperature between 1100 and 1300 ^oC. Moreover, the composite scaffolds with $BaTiO_3$ NPs exhibited accelerated osteoblast attachment even well than that of only HAp and TCP [247]. In another studies, natural and synthetic polymers have been applied with HAp and $BaTiO_3$ NPs to improve the efficacy of the scaffold systems. For example, highly porous $BaTiO_3$ based scaffolds have been fabricated by foam replication process and polarized by using an external electric filed. These scaffolds were coated with gelatin (GEL) and HAp nanostructures and the coated scaffolds exhibited improved compressive strength and elastic modulus as well as remarkably higher cell density of MG63 osteoblast cells compared with the uncoated scaffolds [248]. Further, collagen-HAp/$BaTiO_3$ scaffolds have been explored for their biological influence exhibiting good biomineralization and remarkable osteoinductive properties by Busuioc *et al.* [112] and Zanfir *et al.* [151] in two separate studies. The responsiveness of $BaTiO_3$ towards external stimuli (in the form of electric field) could further be explored to design electric field driven system and should give this fascinating material, edge in tissue engineering and regenerative medicines.

The topography and interconnected pore-network of the scaffold are important factors for

better cellular activities. To obtain these characteristics, uncoated $BaTiO_3$ NPs, Al_2O_3-coated $BaTiO_3$ NPs, and SiO_2-coated $BaTiO_3$ NPs have been incorporated into a poly L/D-lactic acid copolymer (PLDLA) scaffold using breath figure process (dissolving a polymer in a volatile solvent and casting under high humidity conditions). The uncoated $BaTiO_3$ NPs facilitated pore size of 16.2 µm into the scaffold, while both Al_2O_3-coated and SiO_2-coated $BaTiO_3$ NPs based scaffolds showed pore sizes smaller than 5 µm as compared to only PLDLA scaffold (pore size: 1.6 µm). Also, the optimal pore size was obtained in uncoated $BaTiO_3$ NPs incorporated PLDLA scaffold, while retaining the honeycomb-like structure. Moreover, the designed scaffolds were biocompatible to be used potentially for musculoskeletal tissue regeneration [249]. Further, synthetic polymers such as poly(vinyl pyrrolidone) (PVP) and PEG were utilized to prepare cross-linked nanocomposite hydrogels using $BaTiO_3$ NPs and treated with gamma irradiation at different doses (25 and 35 kGy). The obtained hydrogels exhibited good mechanical stimulation and dielectric permittivity was increased with increasing $BaTiO_3$ NPs (1, 2, and 3 wt%) [250].

In addition, Polycaprolactone (PCL)/$BaTiO_3$ piezoelectric composites have been prepared and evaluated under optimal polarization conditions, wherein the composite showed enhanced piezoelectric characteristics with the increasing of $BaTiO_3$ NPs content. The obtained composites exhibited good cell adhesion compared to only PCL, without any cytotoxicity [251]. Furthermore, the piezoelectric nature of PVDF acts a decisive role in rebuilding the endogenous electrical environment of the bone tissue. The more β phase in PVDF directs to greater piezoelectric activity. The β phase nucleation could be induced by incorporating NPs, but the aggregation of NPs can reduce the nucleation ability of the β phase. Therefore, $BaTiO_3$

NPs were hydroxylated and modified with polydopamine (PDA) to accelerate their homogenous dispersion in PVDF Scaffolds. Catechol groups of PDA form hydrogen bonding with hydroxylated-$BaTiO_3$ NPs, whereas amine groups of PDA make bonding with C-F group of PVDF. The functionalized-$BaTiO_3$ NPs remarkably increased the β phase fraction (from 46% to 59%) with an improved output voltage by 356%. Composite scaffold exhibited improved mechanical properties (tensile strength and modulus) and accelerated cell attachment, proliferation, and differentiation [252]. $BaTiO_3$ NPs have been used to prepare piezoelectric composites with widespread applicability not only in tissue engineering but in bioelectronics as well.

In the field of tissue engineering, repair of cartilage tissues is very critical. Cartilage tissue is a type of flexible connective tissue with avascular nature and less systematized microarchitecture. Nanofibrous structure of the scaffold is very promising to mimic the natural structure of the native cartilage. Therefore, poly (3-hydroxybutyrate-co-3-hydroxyvalerate) (PHBV) and $BaTiO_3$ NPs based electrospun scaffolds has been fabricated, wherein the addition of 20% $BaTiO_3$ NPs into the scaffold improved mechanical properties and piezoelectric coefficient of 1.4 pC/N (similar to natural cartilage tissue). Also, electrically polarized scaffolds showed superior cellular activity of human MSCs-derived chondrocytes compared to only PHBV and non-polarized scaffold [253]. In another study, $BaTiO_3$ NPs have been incorporated into alginate as natural polysaccharide to induce osteogenic differentiation of human MSCs. Alginate/ $BaTiO_3$ based 3D scaffold with highly interconnected pore-network and surface nanotopography showed an osteogenic differentiation of cells without adding osteogenic supplements [254]. During joint movement and involvement of mechanical operation, cartilage

tissue experiences electrical potential which also aids in cell regeneration and development. The electric attributes of $BaTiO_3$ NPs could be vital in exploring this environment and develop effective materials for cartilage tissue regeneration.

The field of tissue engineering and regenerative medicine is the need of the hour for an efficient healthcare system. As a potent candidate for tissue regeneration, $BaTiO_3$ NPs should be able to influence the upregulation of specific markers and at the same time should be able to initiate and regulate the mineralization process of extracellular matrix. Further, the ability of $BaTiO_3$ NPs to stimulate the cell differentiation without the inclusion of chemical inducer is another advantage associated with $BaTiO_3$ NPs based systems.

4.3 Biosensors, wearable and implanted bioelectronic devices

Biosensors, wearable and implantable bioelectronics has achieved a great attention and therefore, various wearable and implantable functional bioelectronic devices have widely been developed to improve the quality of life of the patients and healthy persons. However, the continuous operation of these bioelectronic devices is challenging due to the replacement of the conventional batteries in a short time span. In this regard, self-powered bioelectronic devices by using piezoelectric materials (e.g., $BaTiO_3$) have been developed to sensing biomolecules or harvest biomechanical energy from human motions. For example, a self-powered glucose sensor has been fabricated by utilizing $BaTiO_3$ NPs and PVDF, which exhibited promising selectivity, reasonable sensitivity of 23.79 A/mM cm^2, detection limit down to 7.94 M showing linear relationship with glucose concentrations [255]. In a similar study, Su *et al.* investigated $BaTiO_3$ NPs doped PVDF both experimentally and through simulation to elucidate the fundamental mechanism underlying the interfacial coupling effect in the

developed polymer composites to develop high-performance wearable textile bioelectronics [256]. Furthermore, the requirement of flexible and stretchable piezoelectric diagnostic or surgical functional bioelectronic devices for soft and greatly deformable tissues of the human body also poses a substantial challenge. Moreover, self-powered implantable bioelectronic devices are more desirable to provide real-time, precise, and constant monitoring of key physiological or pathological signals (e.g., body temperature, breathing, arterial pulse, heart rate, blood glucose or pressure or oxygen). Also, the power supply in implantable bioelectronic devices is more crucial, wherein the replacement of battery in an implanted device (inside the human body) is highly difficult [257-259]. Among piezoelectric materials, $BaTiO_3$ ceramic NPs has been studied widely due to its non-toxicity, remarkable dielectric and ferroelectric characteristics [174, 260]. In this section, $BaTiO_3$-based piezoelectric wearable and implantable devices are described and discussed.

For wearable electronic devices, poly (vinyl chloride) (PVC)/aligned $BaTiO_3$ nanowires-based flexible hybrid piezoelectric fibre fabric have been developed, which was integrated with copper wires and cotton threads. Here, a 2D fabric like nanogenerator was manufactured where copper wire with interdigital structure functioned as electrode and cotton thread performed the function of a spacer to avert electrode shorting along with the support in increasing the durability of the device **(Figure 9)**. The resemblance of this device with the native fabric like appearance provides edge to this device. Due to the presence of $BaTiO_3$, the device offered the ability to convert the movement of human body into electrical energy. When attached on human arm (for elbow movement), this wearable nanogenerator system could generate 1.9 V output voltage, 24 nA output current and 10.2 nW output power for 80 MΩ as an external load [261].

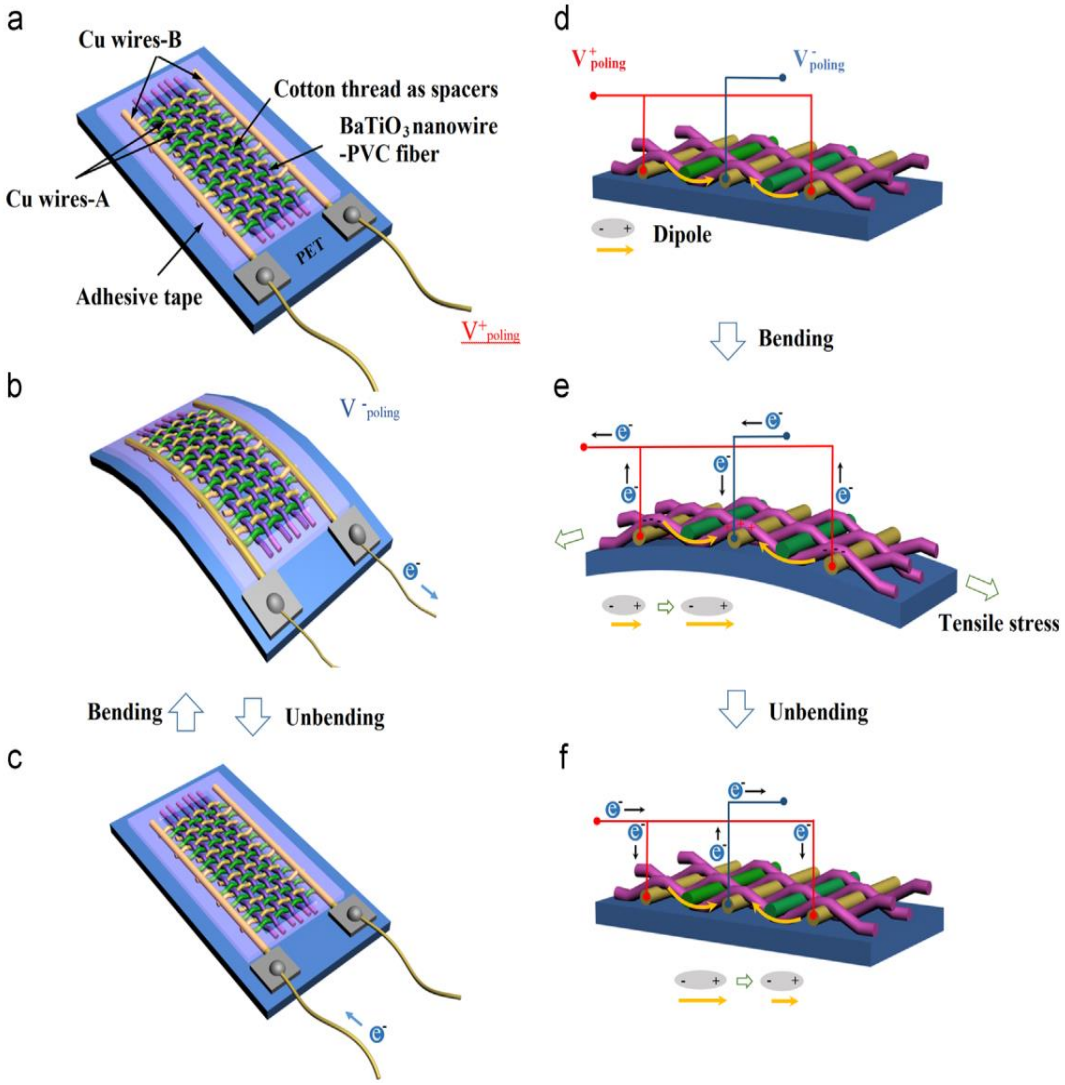

Figure 9. Representations of the operating mechanism of the flexible fabric nanogenerator (FNG). (a) FNG structure, (b) Mechanical deformation (Bending) of FNG along the direction of piezoelectric fibres, (c) Unbending of FNG, (d) The status of FNG after poling process where the dipole aligns alongside the direction of the piezoelectric fibre, (e) Carrier flow due to the generation of piezopotentials on the electrodes under the mechanical bending, and (f) under the

influence of unbending status, the potential disappears with the carriers flowing back. Reproduced with permission. [261] Copyright 2015, Elsevier.

In another study, a $KNaNbO_3$ (lead-free)/$BaTiO_3$ NPs impregnated polydimethylsiloxane (PDMS) flexible composite film-based nanogenerator was prepared and exhibited the efficacy for sleep monitoring or sleep disorder in humans by showing a maximum electrical output 58 V and 450 nA [262]. Powering transient implants using biodegradable power sources is highly promising. Therefore, a biodegradable and biocompatible piezoelectric transducer composed of $BaTiO_3$ NPs and poly (L-lactic-co-glycolic acid) (PLGA) was prepared and used in two different powering arrangements (ultrasonic and energy harvesting from low frequency acoustic waves). The power density of $BaTiO_3$/PLGA transducer reached up to 10 mW/cm2 in ultrasonic powering, while it generated sufficient power for small electronics in low frequency acoustic waves [263]. In a study by Su *et al.*, polydopamine (PDA)-coated $BaTiO_3$ NPs were prepared and PDA@$BaTiO_3$ NPs-doped PVDF fibres were formulated for high-performance wearable bioelectronics (PMNP). Herein, the coating of an optimal volume (2.15 v%) of PDA on $BaTiO_3$ NPs could significantly promote the neighboring *all-trans* conformation in PVDF chains and modulus equivalent at the polymer/nanofiller interface, resulting in the maximum coefficient of piezoelectric charge and voltage as well as mechanical stiffness. Furthermore, the fabricated PMNP exhibited long-term stability, high sensitivity and broad range of pressure sensing, showing a remarkable ability of real-time limb motion detection, identification of facial emotion, respiratory monitoring and human-machine interaction (**Figure 10**) [194]. In another study, fluorinated $BaTiO_3$ (F-$BaTiO_3$)/PVDF-based nanofibrous wearable piezoelectric nanogenerators (PENGs) have been developed and they exhibited three times

higher β-phase content (up to 91%) for 5 wt% F-$BaTiO_3$ than that of $BaTiO_3$ (5 wt%)/PVDF nanofibres. The results exhibited output voltage as high as 1.5 V (under 2N external force) and did not reduce apparently after 300 cycles in a vertical pressing analysis. Also, PENG was observed to be sensitive to detect human motions [264]. These studies reflect the potential of $BaTiO_3$ as a persuasive candidate to develop biosensors and wearable bioelectronics.

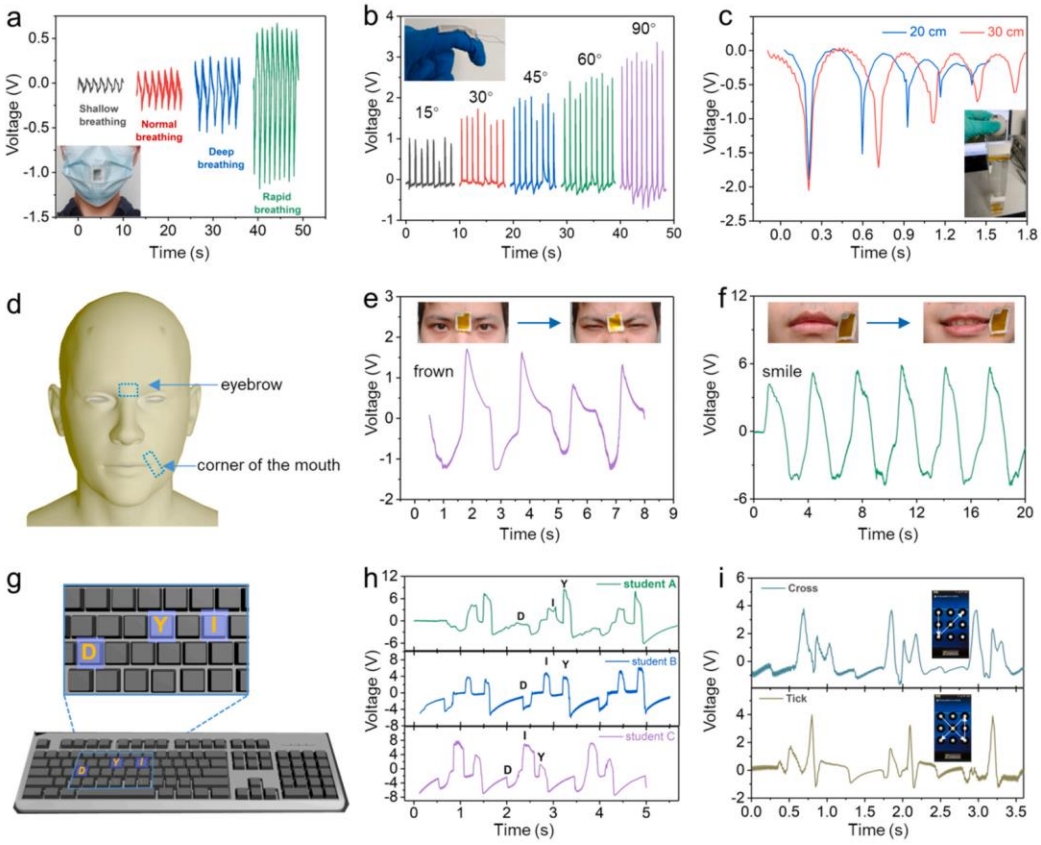

Figure 10. Sensing operation of PMNP textile bioelectronics: (a) Real-time output voltage pattern, (b) dynamic output voltage waveforms of finger bending at different angles, (c) dynamic output pattern for free-falling table tennis ball with various falling heights, and (d) schematic model of PMNP textile bioelectronics for active facial expression identification. Real-time output patterns in response to frown (e) and smile (g). Digital images of PMNP

textiles attached on the keyboard and dynamic voltage patterns of three adult volunteers when typing the word “DIY” (h) and when crossing and ticking on the touchscreen of a smartphone (e) Reproduced with permission. [194] Copyright 2021, Elsevier.

Similarly, a $BaTiO_3$ film-based piezoelectric airflow sensor has been developed unified with PDMS orifice membrane as the core sensing module. Herein, hydrothermally grown $BaTiO_3$ film (on titanium foil) showed an orthorhombic crystal construction with good piezoelectric characteristics. Furthermore, the Young’s modulus and piezoelectric constant of the $BaTiO_3$ film were 100 GPa and 8 pC N^{-1}, respectively. In this study, an algorithm is proposed that determines the sensing performance of the airflow sensor by utilizing the data recorded from the measured piezoelectric signal along with the degree of deflection of the piezoelectric beam. Herein, a relation was established between the pressure and volume rate of airflow across sensing membrane, movement of the piezoelectric sensing beam, and the strain experienced by the piezoelectric film to calculated Young’s modulus and piezoelectric constant of $BaTiO_3$ composite film. With the help of the proposed algorithm and signals produced from the manufactured sensor, significant breath factors of a 20-year-old young male were monitored [265]. One of the requirements for a wearable device is the compact size of the micromachined device, this aspect is adequately addressed using this manufactured system. The manufactured device still has to be evaluated and compared for their efficacy with commercially available breath monitoring systems.

Implantable medical devices exhibit biofilm-related infection issues and cause a main obstacle that limits their effective clinical translation. In this regard, $BaTiO_3$ integrated biomaterial has been developed as anti-infectious medical device (implantable), which demonstrated effective

anti-biofilm activities against Streptococcus mutans without bactericidal outcome by maintaining their mechanical and piezoelectric activities. This anti-adhesive property directed to ~10-fold decrease in colony-forming entities (*in vitro*). The poling process on $BaTiO_3$-nanocomposites caused in asymmetrical surface charge density on each side, which may assist in addressing two main issues in prosthetics such as bacterial contamination and tissue integration. Moreover, $BaTiO_3$-nanocomposites showed excellent biocompatibility towards human gingival fibroblasts and keratinocytes [266] **(Figure 11)**.

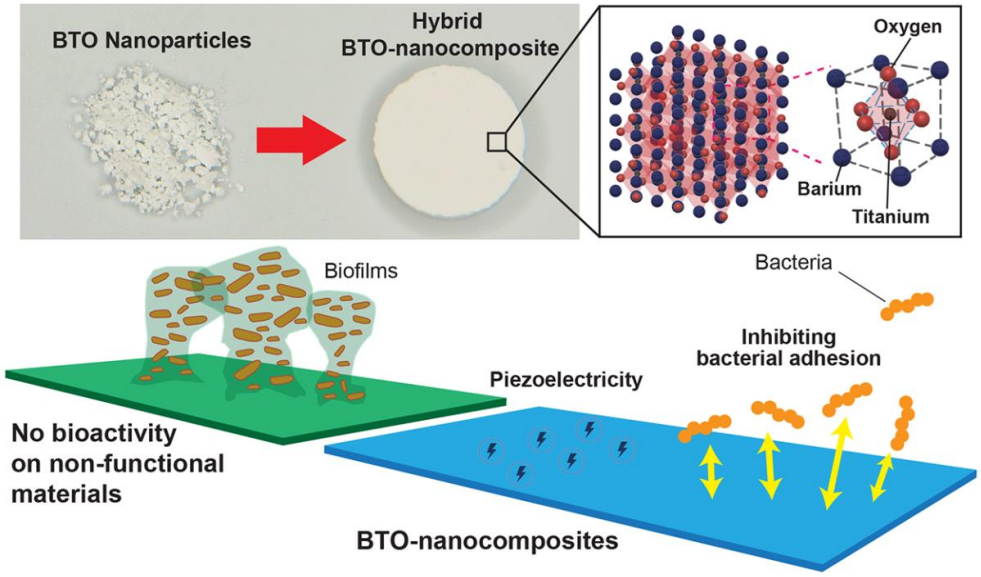

Figure 11. Schematic illustration of a bimodal $BaTiO_3$ nanocomposite platform with antibiofilm and self-powering functionalities Reproduced with permission. [266] Copyright 2021, American Chemical Society.

Neurostimulation is a promising strategy in treating various neurological disorders, wherein intensive miniaturization of neuro-stimulators to millimeter (mm) size dimensions is crucial to avoid invasive surgery or post-surgery trauma and infection [7,8]. The stimulators must also

be able to target nerves located deeper inside the human body (> 5 cm) and require a large average load power (up to some mWs). Therefore, to achieve high output power, large "depth-to-size ratio" (ratio of tissue depth to implant volume), and long-term safety and stability are the main concerns in developing desired stimulators. In this advancement, Charthad *et al*. developed a wireless electrical stimulation implant for peripheral nerves by achieving more than ten times increase in the depth/volume ratio over existing IC-based neurostimulators. The fully integrated implant (size: 2 mm x 3 mm x 6.5 mm, 39 mm^3, and weight: 78 mg) was operated at 10.5 cm in a tissue phantom by using ultrasound for wireless powering (safe intensity level) and co-design strategy (e.g., a miniaturized piezoelectric receiver, IC, off-chip energy storage capacitor, and platinum stimulation electrodes as well as optional blue light emitting diode for promising optogenetic stimulation) for complete operation. As-developed implant system is allowed to externally fully programmable current-regulated stimulation of peripheral nerves, with a broad range of factors both electrical stimulation (amplitude: 22-5000 µA, pulse width: 14-470 µs, and repetition rate: 0-60 Hz) and optical stimulation (optical intensity up to 23 mW/mm^2) as well as high compliance voltage (15 V) for chronic applications. The fully integrated implant, *in vitro* analysis, and the electrical stimulation of a sciatic nerve demonstrated the efficacy of the developed stimulator for peripheral nerves (**Figure 12**) [267].

In the quest of developing advanced wearable electronics associated with biointerface for real time health care monitoring, $BaTiO_3$ NPs have shown to have tremendous potential. Further improvement in the processing methodology, concentration of the initial materials for composite formation, and governing parameters could result in efficient systems for real time

monitoring.

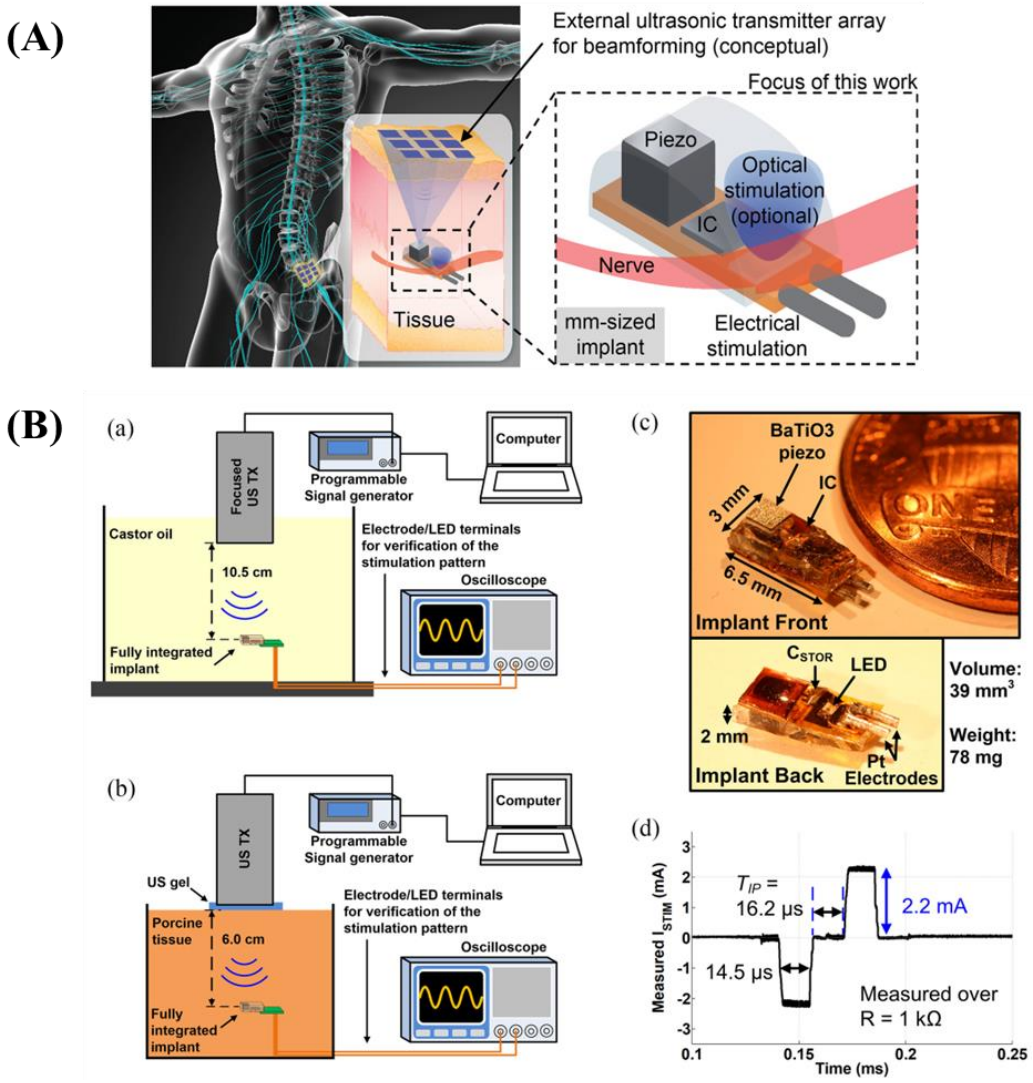

Figure 12. Schematic illustrations of (A) the proposed electrical stimulation implant and (B) the measurement setup for implantable device (fully integrated system) in castor oil in the depth of 10.5 cm (a) and 6 mm of porcine tissue (b), digital image of the fully integrated stimulation system (c), and quantified current waveform (only magnified single pulse is shown) for the setup in (b) and the performance data (discussed in main text) of fully integrated system for the setup in (a). Reproduced from [267].

5. Toxicity assessment and limitations

The translation of nanoparticles based biomedical approaches from *in vitro* assessment to *in vivo* platform may sometimes leads to contradicting results [268]. The administration of nanoparticles *in vivo* aims in treating the targeted pathological condition with minimal harm to the health tissues, hence the toxicity assessment and evaluation of adequate dose rate is a crucial factor which needs a careful examination. Although the underlying mechanism concerning the toxicity of $BaTiO_3$ NPs is still in progress however, oxidative damage due to over production of reactive oxygen species (ROS) have been linked to the underlying toxicity mechanisms of $BaTiO_3$ NPs [117, 269].

In a study, a concentration range of 25-100 µg/mL of $BaTiO_3$ NPs was highlighted to shown decrease in cell viability in case of Human lung cancer cells (A549) with a dose rate of 50 µg/mL of $BaTiO_3$ NPs showing pronounced oxidative stress [117]. Similar results were also presented in a separate study by Staedler *et al.* where a time dependent cytotoxicity of $BaTiO_3$ NPs (50 µg/mL) was evaluated on A549 cells with % cell survival of almost 91%, 84%, and 81% after an exposure of 24 h, 48 h, and 74 h, respectively [270]. The cell survival rate and the dose to be administered is much dependent on the category of cell lines and the exposure time. In this study, the cytotoxicity of $BaTiO_3$ NPs (50 µg/mL) was also evaluated on adenosquamos carcinoma cell line (HTB-178), lung squamous carcinoma cell line (HTB-182), and, nontumoral BEAS-2B cells with different exposure time (24 h, 48 h, and 74 h). Interestingly, at this dose, $BaTiO_3$ NPs did not show extreme cell death with HTB-17B showing the least % cell survival of approximately 74% upon an exposure of 72 h.

Similar results were reported by Bonacino *et al.* in a separate study where a range of harmonic nanoparticles including $BaTiO_3$ NPs were tested for cytotoxicity effect in case of A549, HTB-178, HTB-182, and BEAS-2B cells for an exposure time of 5 h and 24 h [126]. With a dose rate of 50 μg/mL of $BaTiO_3$ NPs a decrease in the cell survival for majority of the cell line was in the range of 20–30%. Further, Genchi *et al.* reported negligible effect on the % live cells while reporting the response of human neuroblastoma cells (SH-SY5Y) towards P(VDF-TrFE)/ $BaTiO_3$ NPs films when compared with control [271].

Although many advantages are associated with $BaTiO_3$ NPs, however adequate flexibility and durability are two aspects that often restricts the single domain use of $BaTiO_3$ NPs [272]. Due to this $BaTiO_3$ NPs is often composited with matrices of many soft polymers and their derivatives [273, 274]. The exact mechanisms of cell responses towards piezoelectric stimulation is still not fully uncovered. There can be multiple factors (type of cells under investigation, mode of functionalization, and size of $BaTiO_3$ NPs) that could affect their internalization, followed pathway and corresponding cellular expressions. In case of $BaTiO_3$ NPs, another factor that limits its biomedical usage is the complexity in differentiating and omitting the cellular responses towards nonspecific phenomenon (mechanical/thermal) that could show overlay effect with the electrical cues [15]. This could lead to misinterpretation of the obtained results, that might affect the clinical translation of $BaTiO_3$ NPs in numerous biomedical applications.

Moreover, the accurate measurement of piezoelectric effect of nanomaterials is another arduous process with piezoresponse force microscopy (PFM) being accepted as the most widely accepted method to detect and quantify piezoelectric behaviour of nanomaterials [275, 276]. However, the piezoelectric effect measured through PFM usually gets influenced by

electrostatic attraction between the sample surface along with resonance frequency associated with the cantilever's tip. These issues could mislead the correct interpretations of the obtained results [277].

In the authors opinion, the overall biological effects of the piezoelectric stimulation by $BaTiO_3$ NPs are assumed to be governed by its subcellular localization. Although, the response of cellular membrane and the participation of voltage-gated channels upon exposure towards piezoelectric simulation have been studied, however, the biochemical pathways triggered, and organelle specific functionalization of $BaTiO_3$ NPs needs in depth investigation.

6. Conclusion

Nanoparticles are considered as the forefront in the advancement of the nanotechnology era thus, selecting the targeted application, curtailing the production cost, and minimizing the long-term health concerns should engage substantial painstaking. The proficiency of nanoparticles is perceived in almost every domain with mounting consideration for their utility in the biomedical applications. The market for nanoparticles commercialization is set to escalate over the next decade with more clinical applications of these nanoparticles are been established. Up recently, the field of nanomedicines have started exploring the intrinsic chemical/physical properties and responses of nanoparticles rather than just using them as a carrier vehicle for delivering therapeutics.

Although there are numerous nanoparticles that have surfaced with some remarkable properties to be utilized for biomedical applications, still the urge to develop novel nanoparticles with superfluous benefits never ends. In this regard, piezoelectric nanomaterials have been explored

for their applicability in bioelectric interface. While $BaTiO_3$ NPs has been studied intensively for the last few decades, there is still a disparity between the accomplished and anticipated performance of this interesting material in terms of biological response. While, substantial amount of evidence at *in vitro* level have been collected so far, in-depth knowledge of the physical mechanisms and biological responses underlying $BaTiO_3$ NPs is still absent.

The clinical translation of $BaTiO_3$ NPs based applications like, cancer therapy, targeted delivery, and cell stimulation needs a comprehensive understanding of its piezoelectric properties, cellular response, optimum dosage, and regulatory response towards internal and external factors. Constant efforts are underway to address every aspect of this fascinating material and with the technological advancement and research efforts, we could observe the transformation of attractive material from lab scale to clinically significant technologies.

7. Future prospectives

In order to interact with biological systems and understand pathological conditions, electrically stimulating cells and tissues has been an important approach being explored. However, the orthodox methods of simulation often need invasive installation of electrodes along with network of wires. This is where $BaTiO_3$ NPs have established its importance by offering the opportunity to provide indirect electrical simulation via mechanically driven simulations. The importance of wireless stimulation of tissues is not only applicable in the treatment process of many diseases but has also been investigated in the field of tissue engineering or regenerative medicine.

Mostly, $BaTiO_3$ NPs has been studied for their ferroelectric behavior that can be used for

bioimaging and biosensing purpose. However, this material could be explored for real time stimulation of heart, muscle, and nerve cells. Further, the property of piezoelectric behavior could find application in cell proliferation and differentiation in close microenvironments. In addition, the high atomic number and high dielectric constant associated with this fascinating material is utilized for enhanced contrast property and cancer therapy however, the toxicity associated with barium is a matter of concern. Although, biomedical applications for $BaTiO_3$ NPs have been reported by many research groups, their biological response, immune modulatory properties, and reliability in cancer therapies has not been explored much. More research efforts should focus on dealing these aspects and challenges. Similarly, more biological application-oriented fabrication of $BaTiO_3$ NPs is required which involves functionalization with peptide sequences, development of nanobiocomposites, and enzyme crosslinked scaffolds. An interdisciplinary approach is essential to evaluate the performance of $BaTiO_3$ NPs using microfluidic chips which will allow to imitate the native architect and physiological attributes of organs/tissues like heart, brain, muscle *etc*., where the utility of $BaTiO_3$ NPs could be evaluated for their cellular behavior.

Overall, $BaTiO_3$ NPs can be considered is a material with some remarkable properties and utility in biomedical field. A thorough understanding of their biological responses could further open new avenues in utilizing this material for advanced clinical applications that would certainly benefit the pharmaceutical and medical sectors.

Declaration of competing interest

The authors declare that they have no known competing financial interests or personal relationships that could have appeared to influence the work reported in this paper.

Acknowledgements

AS, AK and SSH acknowledge the support of National Research Foundation of Korea (NRF) funded by the Ministry of Education, Science and Technology, grant numbers "2021R1I1A3059994, 2020K1A3A1A19088873, 2020R1A6A1AA03044512, and 2020R1A2C1012586". NM, LM and MD acknowledge the support of EIPHI Graduate School (contract ANR-17-EURE-0002), MD acknowledges the support of ANR (contract ANR-21-CE09-0028).

References

1. Sood, A.; Dev, A.; Sardoiwala, M. N.; Choudhury, S. R.; Chaturvedi, S.; Mishra, A. K.; Karmakar, S., *Mat. Sci. Eng. C* **2021,** *129*, 112394.
2. Azharuddin, M.; Zhu, G. H.; Das, D.; Ozgur, E.; Uzun, L.; Turner, A. P. F.; Patra, H. K., *Chem. Commun.* **2019,** *55* (49), 6964-6996.
3. Guigou, C.; Lalande, A.; Millot, N.; Belharet, K.; Bozorg Grayeli, A., *Brain Sci.* **2021,** *11* (3), 358.
4. Kottana, R. K.; Maurizi, L.; Schnoor, B.; Morris, K.; Webb, J. A.; Massiah, M. A.; Millot, N.; Papa, A. L., *Small* **2021,** *17* (1), e2004945.
5. Sood, A.; Arora, V.; Kumari, S.; Sarkar, A.; Kumaran, S. S.; Chaturvedi, S.; Jain, T. K.; Agrawal, G., *Int. J. Biol. Macromol.* **2021,** *189*, 443-454.
6. Kaushik, A., *Expert Opin. Drug Deliv.* **2021,** *18* (5), 531-534.
7. Auría-Soro, C.; Nesma, T.; Juanes-Velasco, P.; Landeira-Viñuela, A.; Fidalgo-Gomez, H.; Acebes-Fernandez, V.; Gongora, R.; Almendral Parra, M. J.; Manzano-Roman, R.; Fuentes, M., *Nanomaterials (Basel, Switzerland)* **2019,** *9* (10), 1365.
8. Wang, W.; Wang, J.; Ding, Y., *J. Mater. Chem. B* **2020,** *8* (22), 4813-4830.
9. Yu, G.; Zhao, X.; Zhou, J.; Mao, Z.; Huang, X.; Wang, Z.; Hua, B.; Liu, Y.; Zhang, F.; He, Z.; Jacobson, O.; Gao, C.; Wang, W.; Yu, C.; Zhu, X.; Huang, F.; Chen, X., *J. Am. Chem. Soc.* **2018,** *140* (25), 8005-8019.
10. Gagliardi, A.; Giuliano, E.; Venkateswararao, E.; Fresta, M.; Bulotta, S.; Awasthi, V.; Cosco, D., *Front. Pharmacol.* **2021,** *12*.
11. Kumar, A.; Sood, A.; Han, S. S., *J. Mater. Chem. B* **2022,** *10* (15), 2761-2780.
12. Zaiter, T.; Cornu, R.; Millot, N.; Herbst, M.; Pellequer, Y.; Moarbess, G.; Martin, H.; Diab-Assaf, M.; Béduneau, A., *Nanotoxicology* **2022**, 1-18.
13. Loiseau, A.; Boudon, J.; Oudot, A.; Moreau, M.; Boidot, R.; Chassagnon, R.; Saïd, N. M.; Roux, S.; Mirjolet, C.; Millot, N., *Cancers (Basel)* **2019,** *11* (12).
14. Balint, R.; Cassidy, N. J.; Cartmell, S. H., *Tissue Eng. Part B Rev.* **2013,** *19* (1), 48-57.
15. Cafarelli, A.; Marino, A.; Vannozzi, L.; Puigmartí-Luis, J.; Pané, S.; Ciofani, G.; Ricotti, L., *ACS Nano* **2021,** *15* (7), 11066-11086.
16. Tai, G.; Tai, M.; Zhao, M., *Burns Trauma* **2018,** *6* (1), 20.
17. Moarefian, M.; Davalos, R. V.; Burton, M. D.; Jones, C. N., *Front. Immunol.* **2021,** *12*,

674727-674727.

18. Hotary, K. B.; Robinson, K. R., *Dev. Biol.* **1994,** *166* (2), 789-800.

19. Kapat, K.; Shubhra, Q. T. H.; Zhou, M.; Leeuwenburgh, S., *Adv. Funct. Mater.* **2020,** *30* (44), 1909045.

20. Marino, A.; Genchi, G. G.; Sinibaldi, E.; Ciofani, G., *ACS Appl. Mater. Interfaces* **2017,** *9* (21), 17663-17680.

21. Xu, Q.; Gao, X.; Zhao, S.; Liu, Y.-N.; Zhang, D.; Zhou, K.; Khanbareh, H.; Chen, W.; Zhang, Y.; Bowen, C., *Adv. Mater.* **2021,** *33* (27), 2008452.

22. Ma, J.; Li, T.; Chen, Y. H.; Lim, T. H.; Boey, F. Y. C., *Key Eng. Mater.* **2007,** *334-335*, 1117-1120.

23. Chen, Y.; Xiong, M.; Dong, Y.; Haberman, A.; Cao, J.; Liu, H.; Zhou, W.; Zhang, S.-C., *Cell stem cell* **2016,** *18* (6), 817-826.

24. Auffenberg, E.; Jurik, A.; Mattusch, C.; Stoffel, R.; Genewsky, A.; Namendorf, C.; Schmid, R. M.; Rammes, G.; Biel, M.; Uhr, M., *Sci. Rep.* **2016,** *6* (1), 1-11.

25. Lau, C.-P.; Siu, C.-W.; Tse, H.-F., *Circulation* **2014,** *129* (7), 811-822.

26. Qian, L.; Huang, Y.; Spencer, C. I.; Foley, A.; Vedantham, V.; Liu, L.; Conway, S. J.; Fu, J. D.; Srivastava, D., *Nature* **2012,** *485* (7400), 593-8.

27. Bettinger, C. J.; Bruggeman, J. P.; Misra, A.; Borenstein, J. T.; Langer, R., *Biomaterials* **2009,** *30* (17), 3050-7.

28. Shin, D.-M.; Hong, S. W.; Hwang, Y.-H., *Nanomaterials (Basel, Switzerland)* **2020,** *10* (1), 123.

29. Chorsi, M. T.; Curry, E. J.; Chorsi, H. T.; Das, R.; Baroody, J.; Purohit, P. K.; Ilies, H.; Nguyen, T. D., *Adv. Mater.* **2019,** *31* (1), e1802084.

30. Jiang, J.; Pi, J.; Cai, J., *Bioinorg. Chem. Appl.* **2018,** *2018*, 1062562.

31. Zhang, Y.; Nayak, T. R.; Hong, H.; Cai, W., *Curr. Mol. Med.* **2013,** *13* (10), 1633-1645.

32. Turhan, E. A.; Pazarçeviren, A. E.; Evis, Z.; Tezcaner, A., *Nanotechnology* **2022,** *33* (24), 242001.

33. Farshid, B.; Lalwani, G.; Shir Mohammadi, M.; Simonsen, J.; Sitharaman, B., *J. Biomed. Mater. Res. B Appl. Biomater.* **2017,** *105* (2), 406-419.

34. Sruthi, S.; Nury, T.; Millot, N.; Lizard, G., *Environ. Sci. Pollut. Res. Int.* **2021,** *28* (10), 12500-12520.

35. Sruthi, S.; Millot, N.; Mohanan, P. V., *Int. J. Biol. Macromol.* **2017,** *103*, 808-818.

36. Bai, R.; Sun, Q.; He, Y.; Peng, L.; Zhang, Y.; Zhang, L.; Lu, W.; Deng, J.; Zhuang, Z.; Yu, T.; Wei, Y., *Front. Bioeng. Biotechnol.* **2022,** *10*.

37. Rieu, J.; Goeuriot, P., *Clin. Mater.* **1993,** *12* (4), 211-7.

38. Genchi, G. G.; Marino, A.; Rocca, A.; Mattoli, V.; Ciofani, G., *Nanotechnology* **2016,** *27* (23), 232001.

39. Yoon, Y. N.; Lee, D.-S.; Park, H. J.; Kim, J.-S., *Sci. Rep.* **2020,** *10* (1), 2560.

40. Ciofani, G.; Danti, S.; D'Alessandro, D.; Moscato, S.; Petrini, M.; Menciassi, A., *Nanoscale Res. Lett.* **2010,** *5* (7), 1093.

41. Dempsey, C.; Lee, I.; Cowan, K. R.; Suh, J., *Colloids Surf. B* **2013,** *112*, 108-112.

42. Joulaud, C.; Mugnier, Y.; Djanta, G.; Dubled, M.; Marty, J.-C.; Galez, C.; Wolf, J.-P.; Bonacina, L.; Le Dantec, R., *J. Nanobiotechnol.* **2013,** *11* (1), S8.

43. Le Dantec, R.; Mugnier, Y.; Djanta, G.; Bonacina, L.; Extermann, J.; Badie, L.; Joulaud, C.; Gerrmann, M.; Rytz, D.; Wolf, J. P.; Galez, C., *J. Phys. Chem. C* **2011,** *115* (31), 15140-15146.

44. Zaki, N. A. F.; Aziz, A. A.; Khairudin, N.; Burham, N. In *Simulation of Zinc Oxide, Barium Sodium Niobate, and Barium Titanate as Lead-Free Piezoelectric Materials*, 2021 IEEE Regional Symposium on Micro and Nanoelectronics (RSM), 2-4 Aug. 2021; **2021**; pp 38-41.

45. Jarkov, V.; Allan, S. J.; Bowen, C.; Khanbareh, H., *Int. Mater. Rev.* **2022,** *67* (7), 683-733.

46. Wainer, E., *Trans. Electrochem. Soc.* **1946,** *89* (1), 331.

47. Waku, T. O. a. S., *Splendid Tita-Bari [in Japanese], Maruzen, Tokyo* **1990**.

48. Randall, C. A., Newnham, R.E., Cross, L.E, **2004**.

49. Wul, B. M., Goldman, I.M., , *C. r. hebd. séances Acad. sci.* **1945,** *46*, 139-142.

50. von Hippel, A., Breckenridge, R.G., Chesley, F.G., Tisza, L, *Ind. Eng. Chem.* **1946,** *38*, 1097–1109.

51. B. Jaffe , W. C. a. H. J., *Academic Press , London* **1971**.

52. S. Roberts, *Phys. Rev.* **1947,** *71* 890 – 895

53. Rooksby, H. P., *Nature* **1945,** *155*, 484.

54. Megaw, H. D., *Nature* **1945,** *155*, 484-485.

55. F. Jona, G. S., *Dover Publications, INC., New York* **1993**.

56. Kwei, G. H.; Lawson, A. C.; Billinge, S. J. L.; Cheong, S. W., *J. Phys. Chem.* **1993,** *97*

(10), 2368-2377.

57. Frey, M. H.; Payne, D. A., *Phys. Rev. B* **1996,** *54* (5), 3158-3168.

58. Perriat, P.; Niepce, J. C.; Caboche, G., *J. Therm. Anal.* **1994,** *41* (2), 635-649.

59. Goswami, A. K., *J. Appl. Phys.* **1969,** *40* (2), 619-624.

60. Tan, Y.; Zhang, J.; Wu, Y.; Wang, C.; Koval, V.; Shi, B.; Ye, H.; McKinnon, R.; Viola, G.; Yan, H., *Sci. Rep.* **2015,** *5* (1), 9953.

61. Kinoshita, K.; Yamaji, A., *J. Appl. Phys.* **1976,** *47* (1), 371-373.

62. Reavley, M. J.-H.; Guo, H.; Yuan, J.; Ng, A. Y. R.; Ho, T. Y. K.; Tan, H. T.; Du, Z.; Gan, C. L., *J. Eur. Ceram. Soc.* **2022,** *42* (12), 4934-4943.

63. Harwood, M. G.; Popper, P.; Rushman, D. F., *Nature* **1947,** *160* (4054), 58-59.

64. Petrovsky, V.; Petrovsky, T.; Kamlapurkar, S.; Dogan, F., *J. Am. Ceram. Soc.* **2008,** *91* (11), 3590-3592.

65. Buscaglia, V.; Randall, C. A., *J. Eur. Ceram. Soc.* **2020,** *40* (11), 3744-3758.

66. Zhao, Z.; Buscaglia, V.; Viviani, M.; Buscaglia, M. T.; Mitoseriu, L.; Testino, A.; Nygren, M.; Johnsson, M.; Nanni, P., *Phys. Rev. B* **2004,** *70* (2), 024107.

67. Imanaga, S.; Miura, K., *Jpn. J. Appl. Phys.* **2012,** *51*, 031502.

68. Deng, X.; Wang, X.; Wen, H.; Chen, L.; Chen, L.; Li, L., *Appl. Phys. Lett.* **2006,** *88* (25), 252905.

69. Xu, H.; Gao, L.; Guo, J., *J. Eur. Ceram. Soc.* **2002,** *22* (7), 1163-1170.

70. Xu, H.; Gao, L., **2003,** *86* (1), 203-205.

71. Chen, K.-Y.; Chen, Y.-W., *Powder Technol.* **2004,** *141* (1), 69-74.

72. Sun, W.; Liu, W.; Li, J., *Powder Technol.* **2006,** *166* (2), 55-59.

73. Zheng, H.; Zhu, K.; Wu, Q.; Liu, J.; Qiu, J., *J. Cryst. Growth* **2013,** *363*, 300-307.

74. Kwon, S.-G.; Park, B.-H.; Choi, K.; Choi, E.-S.; Nam, S.; Kim, J.-W.; Kim, J.-H., *J. Eur. Ceram. Soc.* **2006,** *26* (8), 1401-1404.

75. Viswanath, R. N.; Ramasamy, S., *Nanostructured Mater.* **1997,** *8* (2), 155-162.

76. Kavian, R.; Saidi, A., *J. Alloys Compd.* **2009,** *468* (1), 528-532.

77. Kim, S.; Lee, M.; Noh, T.; Lee, C., *J. Mater. Sci.* **1996,** *31* (14), 3643-3645.

78. Shi, A.-h.; Yan, W.-b.; Li, Y.-j.; Huang, K.-l., *J. Cent. South Univ. Technol.* **2008,** *15* (3), 334-338.

79. Jung, W.-S.; Park, J.; Park, Y.; Yoon, D.-H., *Ceram. Int.* **2010,** *36* (6), 1997-2002.

80. Maison, W.; Kleeberg, R.; Heimann, R. B.; Phanichphant, S., *J. Eur. Ceram. Soc.* **2003,**

23 (1), 127-132.

81. Culic-Viskota, J.; Dempsey, W. P.; Fraser, S. E.; Pantazis, P., *Nat. Protoc.* **2012,** *7* (9), 1618-33.

82. Madzharova, F.; Nodar, Á.; Živanović, V.; Huang, M. R. S.; Koch, C. T.; Esteban, R.; Aizpurua, J.; Kneipp, J., **2019,** *29* (49), 1904289.

83. Jordan, T.; O'Brien, M. A.; Spatarelu, C.-P.; Luke, G. P., *ACS Appl. Nano Mater.* **2020,** *3* (3), 2636-2646.

84. Ciofani, G.; Danti, S.; D'Alessandro, D.; Moscato, S.; Petrini, M.; Menciassi, A., *Nanoscale Res. Lett.* **2010,** *5* (7), 1093-101.

85. Hoshina, T.; Wada, S.; Kuroiwa, Y.; Tsurumi, T., *Appl. Phys. Lett.* **2008,** *93* (19), 192914.

86. Ciofani, G.; Danti, S.; D'Alessandro, D.; Ricotti, L.; Moscato, S.; Bertoni, G.; Falqui, A.; Berrettini, S.; Petrini, M.; Mattoli, V.; Menciassi, A., *ACS Nano* **2010,** *4* (10), 6267-6277.

87. Rajabi, A. H.; Jaffe, M.; Arinzeh, T. L., *Acta Biomater.* **2015,** *24*, 12-23.

88. Joshi, U. A.; Lee, J. S., *Small* **2005,** *1* (12), 1172-1176.

89. O'Brien, S.; Brus, L.; Murray, C. B., *J. Am. Chem. Soc.* **2001,** *123* (48), 12085-12086.

90. Jiang, B.; Pang, X.; Li, B.; Lin, Z., *J. Am. Chem. Soc.* **2015,** *137* (36), 11760-11767.

91. Deng, Z.; Dai, Y.; Chen, W.; Pei, X.; Liao, J., *Nanoscale Res. Lett.* **2010,** *5* (7), 1217.

92. Qiu, J. H.; Ding, J. N.; Yuan, N. Y.; Cao, H. X.; Wang, X. Q.; Zhou, Y., *J. Appl. Phys.* **2011,** *109* (5), 054103.

93. Adireddy, S.; Lin, C.; Cao, B.; Zhou, W.; Caruntu, G., *Chem. Mater.* **2010,** *22* (6), 1946-1948.

94. Urban, J. J.; Yun, W. S.; Gu, Q.; Park, H., *J. Am. Chem. Soc.* **2002,** *124* (7), 1186-7.

95. Damjanovic, D., *Rep. Prog. Phys.* **1998,** *61* (9), 1267-1324.

96. Hong, J.; Fang, D., *Appl. Phys. Lett.* **2008,** *92* (1), 012906.

97. Zhong, W. L.; Wang, Y. G.; Zhang, P. L.; Qu, B. D., *Phys. Rev. B* **1994,** *50* (2), 698-703.

98. Pertsev, N. A.; Zembilgotov, A. G.; Tagantsev, A. K., *Phys. Rev. Lett.* **1998,** *80* (9), 1988-1991.

99. Zhang, Y.; Hong, J.; Liu, B.; Fang, D., *Nanotechnology* **2009,** *21* (1), 015701.

100. Li, W.; Yang, T.; Liu, C.; Huang, Y.; Chen, C.; Pan, H.; Xie, G.; Tai, H.; Jiang, Y.; Wu, Y.; Kang, Z.; Chen, L.-Q.; Su, Y.; Hong, Z., *Adv. Sci.* **2022,** *9* (13), 2105550.

101. Beier, C. W.; Cuevas, M. A.; Brutchey, R. L., *Langmuir* **2010,** *26* (7), 5067-5071.

102. Kim, P.; Jones, S. C.; Hotchkiss, P. J.; Haddock, J. N.; Kippelen, B.; Marder, S. R.; Perry,

J. W., *Adv. Mater.* **2007,** *19* (7), 1001-1005.
103. Park, M. B.; Cho, N. H., *Appl. Surf. Sci.* **2005,** *244* (1-4), 418-421.
104. Wang, Y.; Yao, M.; Ma, R.; Yuan, Q.; Yang, D.; Cui, B.; Ma, C.; Liu, M.; Hu, D., *J. Mater. Chem. A* **2020,** *8* (3), 884-917.
105. Niu, Y.; Bai, Y.; Yu, K.; Wang, Y.; Xiang, F.; Wang, H., *ACS Appl. Mater. Interfaces* **2015,** *7* (43), 24168-24176.
106. Morsi, M. A.; Abdelrazek, E. M.; Ramadan, R. M.; Elashmawi, I. S.; Rajeh, A., *Polym. Testing* **2022,** *114*, 107705.
107. Wei, X. F.; Li, W. Z.; Chen, H. F.; Lv, M.; Wang, H. W.; Qi, X. W., *J. Phys.: Conf. Series* **2022,** *2194* (1), 012045.
108. Bouharras, F. E.; Raihane, M.; Ameduri, B., *Prog. Mater. Sci.* **2020,** *113*, 100670.
109. Torabi, A.; Jafari, S. H.; Khonakdar, H. A.; Goodarzi, V.; Yu, L.; Altstädt, V.; Skov, A. L., *J. Polym. Res.* **2022,** *29* (10), 425.
110. Lee, S. H.; Choi, Y. C.; Kim, M. S.; Ryu, K. M.; Jeong, Y. G., *Fibers Polym.* **2020,** *21* (3), 473-479.
111. Kim, P.; Doss, N. M.; Tillotson, J. P.; Zhang, X.-H.; Jones, S. C.; Hotchkiss, P. J.; Li, J.; Calame, J. P.; Domercq, B.; Kippelen, B.; Marder, S. R.; Perry, J. W., *MRS Online Proceedings Library* **2009,** *1113* (1), 205.
112. Busuioc, C.; Voicu, G.; Jinga, S.-I.; Mitran, V.; Cimpean, A., *Mater. Lett.* **2019,** *253*, 317-322.
113. Wu, C.; Tang, Y.; Zhao, K.; Jiao, M.; Wu, Z., *Micro Nano Lett.* **2020,** *15* (7), 421-424.
114. Shah, A. A.; Khan, A.; Dwivedi, S.; Musarrat, J.; Azam, A., *Mater. Lett.* **2018,** *229*, 130-133.
115. Sasikumar, M.; Ganeshkumar, A.; Chandraprabha, M. N.; Rajaram, R.; Krishna, R. H.; Ananth, N.; Sivakumar, P., *Mater. Res. Exp.* **2018,** *6* (2), 025408.
116. Boschetto, F.; Doan, H. N.; Phong Vo, P.; Zanocco, M.; Yamamoto, K.; Zhu, W.; Adachi, T.; Kinashi, K.; Marin, E.; Pezzotti, G., *Molecules* **2021,** *26* (10).
117. Ahamed, M.; Akhtar, M. J.; Khan, M. A. M.; Alhadlaq, H. A.; Alshamsan, A., *Nanomaterials (Basel)* **2020,** *10* (11).
118. Candito, M.; Simoni, E.; Gentilin, E.; Martini, A.; Marioni, G.; Danti, S.; Astolfi, L., *Int. J. Mol. Sci.* **2022,** *23* (3).
119. Donati, G., *Nat. Photon.* **2016,** *10* (8), 498-498.

120. Ma, C.; Yan, J.; Wei, Y.; Liu, P.; Yang, G., *J. Mater. Chem. C* **2017,** *5* (19), 4810-4819.
121. Fejer, M. M.; Magel, G. A.; Jundt, D. H.; Byer, R. L., *IEEE J. Quant. Electron.* **1992,** *28* (11), 2631-2654.
122. Bouhelier, A.; Beversluis, M.; Hartschuh, A.; Novotny, L., *Phys. Rev. Lett.* **2003,** *90* (1), 013903.
123. Liu, S.; Keeler, G. A.; Reno, J. L.; Sinclair, M. B.; Brener, I., *Adv. Opt. Mater.* **2016,** *4* (10), 1457-1462.
124. Zhang, S.; Jiang, R.; Xie, Y.-M.; Ruan, Q.; Yang, B.; Wang, J.; Lin, H.-Q., *Adv. Mater.* **2015,** *27* (45), 7432-7439.
125. Kim, E.; Steinbrück, A.; Buscaglia, M. T.; Buscaglia, V.; Pertsch, T.; Grange, R., *ACS Nano* **2013,** *7* (6), 5343-5349.
126. Bonacina, L., *Mol. Pharma.* **2013,** *10* (3), 783-792.
127. Huang, R. H.; Sobol, N. B.; Younes, A.; Mamun, T.; Lewis, J. S.; Ulijn, R. V.; O'Brien, S., *ACS Appl. Mater. Interfaces* **2020,** *12* (46), 51135-51147.
128. Ashton, J. R.; West, J. L.; Badea, C. T., *Front. Pharmacol.* **2015,** *6*, 256.
129. Khoeini, M.; Kolahi, A.; Hesaraki, S., *Ceram. Int.* **2022,** *48* (6), 7643-7651.
130. Stimphil, E.; Nagesetti, A.; Guduru, R.; Stewart, T.; Rodzinski, A.; Liang, P.; Khizroev, S., *Appl. Phys. Rev.* **2017,** *4* (2), 021101.
131. Pandey, P.; Ghimire, G.; Garcia, J.; Rubfiaro, A.; Wang, X.; Tomitaka, A.; Nair, M.; Kaushik, A.; He, J., *ACS Sensors* **2021,** *6* (2), 340-347.
132. Stewart, T. S.; Nagesetti, A.; Guduru, R.; Liang, P.; Stimphil, E.; Hadjikhani, A.; Salgueiro, L.; Horstmyer, J.; Cai, R.; Schally, A.; Khizroev, S., *Nanomedicine* **2018,** *13* (4), 423-438.
133. Rao, B. N.; Kaviraj, P.; Vaibavi, S. R.; Kumar, A.; Bajpai, S. K.; Arockiarajan, A., *J. Appl. Phys.* **2017,** *122* (16), 164102.
134. Guduru, R.; Liang, P.; Runowicz, C.; Nair, M.; Atluri, V.; Khizroev, S., *Sci. Rep.* **2013,** *3* (1), 2953.
135. Goldberg, E.; Suárez, C.; Alfonso, M.; Marchese, J.; Soba, A.; Marshall, G., *Bioelectrochemistry* **2018,** *124*, 28-39.
136. Angelats-Silva, L. M.; Pérez-Azahuanche, F.; Roldan-Lopez, J. A.; Emelianov, N. A.; Céspedes-Vásquez, R. B.; Valverde-Alva, M. A., *MRS Adv.* **2022,** *7* (12), 260-264.
137. Papa, A.-L.; Dumont, L.; Vandroux, D.; Millot, N., *Nanotoxicology* **2012,** *7* (6), 1131-

1142.
138. Sabourian, P.; Yazdani, G.; Ashraf, S. S.; Frounchi, M.; Mashayekhan, S.; Kiani, S.; Kakkar, A., *Int. J. Mol. Sci.* **2020,** *21* (21), 8019.
139. Singh, N.; Marets, C.; Boudon, J.; Millot, N.; Saviot, L.; Maurizi, L., *Nanoscale Adv.* **2021,** *3* (5), 1209-1229.
140. Qi, J. Q.; Sun, L.; Wang, Y.; Chen, W. P.; Du, P.; Xu, Y. G.; Li, L. T.; Nan, C. W.; Chan, H. L. W., *Adv. Powder Technol.* **2011,** *22* (3), 401-404.
141. Seeharaj, P.; Boonchom, B.; Charoonsuk, P.; Kim-Lohsoontorn, P.; Vittayakorn, N., *Ceram. Int.* **2013,** *39*, S559-S562.
142. Baeten, F.; Derks, B.; Coppens, W.; van Kleef, E., *J. Eur. Ceram. Soc.* **2006,** *26* (4), 589-592.
143. Chen, X.; Chao, X.; Yang, Z., *Mater. Res. Bull.* **2019,** *111*, 259-266.
144. Moghtada, A.; Ashiri, R., *Ultrasonics Sonochemistry* **2018,** *41*, 127-133.
145. Song, Y.-L.; Liu, X.-L.; Zhang, J.-Q.; Zou, X.-Y.; Chen, J.-F., *Powder Technol.* **2005,** *155* (1), 26-32.
146. Chen, J.-F.; Shen, Z.-G.; Liu, F.-T.; Liu, X.-L.; Yun, J., *Scripta Mater.* **2003,** *49* (6), 509-514.
147. Salazar-Kuri, U.; Estevez, J. O.; Silva-González, N. R.; Pal, U.; Mendoza, M. E., *J. Magn. Magn. Mater.* **2017,** *442*, 247-254.
148. Giannakoudakis, D. A.; Pearsall, F.; Florent, M.; Lombardi, J.; O'Brien, S.; Bandosz, T. J., *J. Colloid and Interface Sci.* **2018,** *531*, 233-244.
149. Fuentes, S.; Dubo, J.; Barraza, N.; González, R.; Veloso, E., *J. Magn. Magn. Mater.* **2015,** *377*, 65-69.
150. Prado, L. R.; de Resende, N. S.; Silva, R. S.; Egues, S. M. S.; Salazar-Banda, G. R., *Chem. Eng. Process.* **2016,** *103*, 12-20.
151. Zanfir, A. V.; Voicu, G.; Busuioc, C.; Jinga, S. I.; Albu, M. G.; Iordache, F., *Mater. Sci. Eng. C* **2016,** *62*, 795-805.
152. Sadeghzadeh Attar, A.; Salehi Sichani, E.; Sharafi, S., *J. Mater. Res. Technol.* **2017,** *6* (2), 108-115.
153. Komarneni, S.; Katsuki, H., *Ceram. Int.* **2010,** *36* (3), 1165-1169.
154. Jiao, H.; Zhao, K.; Ma, L.; Tang, Y.; Liu, X.; Bian, T., *J. Alloys Compd.* **2017,** *693*, 221-225.

155. Lin, S.-W.; Qian, W.-H.; Huo, H.-J.; Li, B.-Z.; Li, Y.; Yang, Y.-G., *Chin. Chem. Lett.* **2017,** *28* (5), 1111-1113.

156. Rath, M. K.; Pradhan, G. K.; Pandey, B.; Verma, H. C.; Roul, B. K.; Anand, S., *Mater. Lett.* **2008,** *62* (14), 2136-2139.

157. Ma, Q.; Mimura, K.-i.; Kato, K., *J. Alloys Compd* **2016,** *655*, 71-78.

158. Reverón, H.; Elissalde, C.; Aymonier, C.; Bidault, O.; Maglione, M.; Cansell, F., *J. Nanosci. Nanotechnol.* **2005,** *5* (10), 1741-4.

159. Reverón, H.; Aymonier, C.; Loppinet-Serani, A.; Elissalde, C.; Maglione, M.; Cansell, F., *Nanotechnology* **2005,** *16* (8), 1137-1143.

160. Zhang, Y.; Wang, L.; Xue, D., *Powder Technol.* **2012,** *217*, 629-633.

161. Sundararajan, T.; Prabu, S. B.; Vidyavathy, S. M., *Mater. Res. Bull.* **2012,** *47* (6), 1448-1454.

162. Stojanovic, B. D.; Simoes, A. Z.; Paiva-Santos, C. O.; Jovalekic, C.; Mitic, V. V.; Varela, J. A., *J. Eur. Ceram. Soc.* **2005,** *25* (12), 1985-1989.

163. Ren, P.; Fan, H.; Wang, X.; Shi, J., *J. Alloys Compd.* **2011,** *509* (22), 6423-6426.

164. Ashiri, R.; Heidary Moghadam, A.; Ajami, R., *J. Alloys Compd.* **2015,** *648*, 265-268.

165. Ohara, S.; Kondo, A.; Shimoda, H.; Sato, K.; Abe, H.; Naito, M., *Mater. Lett.* **2008,** *62* (17), 2957-2959.

166. Sundararajan, T.; Balasivanandha Prabu, S., *Mater. Chem. Phys.* **2013,** *139* (2), 465-470.

167. Marković, S.; Mitrić, M.; Starčević, G.; Uskoković, D., *Ultrason. Sonochem.* **2008,** *15* (1), 16-20.

168. Purwanto, A.; Wang, W.-N.; Lenggoro, I. W.; Okuyama, K., *J. Eur. Ceram. Soc.* **2007,** *27* (16), 4489-4497.

169. Chen, Y.-Y.; Yu, B.-Y.; Wang, J.-H.; Cochran, R. E.; Shyue, J.-J., *Inorg. Chem.* **2009,** *48* (2), 681-686.

170. Yuh, J.; Nino, J. C.; Sigmund, W. M., *Mater. Lett.* **2005,** *59* (28), 3645-3647.

171. Zanfir, A. V.; Voicu, G.; Jinga, S. I.; Vasile, E.; Ionita, V., *Ceram. Int.* **2016,** *42* (1, Part B), 1672-1678.

172. Millot, N.; Begin-Colin, S.; Perriat, P.; Le Caër, G., *J. Solid State Chem.* **1998,** *139* (1), 66-78.

173. Guigue-Millot, N.; Bégin-Colin, S.; Champion, Y.; Hÿtch, M. J.; Le Caër, G.; Perriat, P.,

J. Solid State Chem. **2003,** *170* (1), 30-38.

174. Jiang, B.; Iocozzia, J.; Zhao, L.; Zhang, H.; Harn, Y.-W.; Chen, Y.; Lin, Z., *Chem. Soc. Rev.* **2019,** *48* (4), 1194-1228.

175. Zhao, J.; Wang, X.; Chen, R.; Li, L., *Ceram. Int.* **2007,** *33* (2), 207-212.

176. Ho, T.-H.; Chang, S.-J.; Li, C.-C., *Mater. Chem. Phys.* **2016,** *172*, 1-5.

177. Moharana, S.; Chopkar, M. K.; Mahaling, R. N., *J. Electron. Mater.* **2020,** *49* (7), 4272-4281.

178. Guan, S.; Yaokai, T.; Song, S.; Liu, H.; Zhao, S., *Mater. Sci. Eng. B-Adv. Funct. Solid-State Mater.* **2021,** *271*, 115280.

179. Chang, S.-J.; Liao, W.-S.; Ciou, C.-J.; Lee, J.-T.; Li, C.-C., *J. Colloid Interface Sci.* **2009,** *329* (2), 300-305.

180. Li, C.-C.; Chang, S.-J.; Lee, J.-T.; Liao, W.-S., *Colloids Surf. A Physicochem. Eng. Aspects* **2010,** *361* (1), 143-149.

181. Ahangaran, F.; Navarchian, A. H., *Adv. Colloid Interface Sci.* **2020,** *286*, 102298.

182. Pujari, S. P.; Scheres, L.; Marcelis, A. T. M.; Zuilhof, H., *Angew. Chem. Int. Ed.* **2014,** *53* (25), 6322-6356.

183. Wattendorf, U.; Merkle, H. P., *J. Pharm. Sci.* **2008,** *97* (11), 4655-69.

184. Bulte, J. W.; de Cuyper, M.; Despres, D.; Frank, J. A., *J. Magn. Reson. Imaging* **1999,** *9* (2), 329-35.

185. Taheri, M.; Maaref, S.; Kantzas, A.; Bryant, S.; Trudel, S., *Chem. Phys.* **2023,** *564*, 111701.

186. Daou, T. J.; Pourroy, G.; Greneche, J. M.; Bertin, A.; Felder-Flesch, D.; Begin-Colin, S., *Dalton Transact.* **2009,** (23), 4442-4449.

187. Beak, K.; Choi, M.; Kim, D. H.; Yu, Y.; Theerthagiri, J.; Al-Mohaimeed, A. M.; Kim, Y.; Jung, H. J.; Choi, M. Y., *Chemosphere* **2022,** *286*, 131734.

188. Pązik, R.; Andersson, R.; Kępiński, L.; Nedelec, J.-M.; Kessler, V. G.; Seisenbaeva, G. A., *J. Phys. Chem. C* **2011,** *115* (20), 9850-9860.

189. Maji, M.; Kivale, P.; Ghosh, M., *J. Drug Deliv. Sci. Technol.* **2022,** *75*, 103617.

190. Tawade, B. V.; Apata, I. E.; Singh, M.; Das, P.; Pradhan, N.; Al-Enizi, A. M.; Karim, A.; Raghavan, D., *Nanotechnology* **2021,** *32* (14), 142004.

191. Zamperlin, N.; Bottacini, A.; Callone, E.; Pegoretti, A.; Fontana, M.; Dirè, S., *Molecules* **2022,** *27* (19), 6499.

192. Yan, X.; Cao, W.; Li, H., *Materials (Basel)* **2021,** *15* (1).
193. Su, Y.; Chen, C.; Pan, H.; Yang, Y.; Chen, G.; Zhao, X.; Li, W.; Gong, Q.; Xie, G.; Zhou, Y.; Zhang, S.; Tai, H.; Jiang, Y.; Chen, J., *Adv. Funct. Mater.* **2021,** *31* (19), 2010962.
194. Su, Y.; Li, W.; Yuan, L.; Chen, C.; Pan, H.; Xie, G.; Conta, G.; Ferrier, S.; Zhao, X.; Chen, G., *Nano Energy* **2021,** *89*, 106321.
195. Wang, Y.; Barhoumi, A.; Tong, R.; Wang, W.; Ji, T.; Deng, X.; Li, L.; Lyon, S. A.; Reznor, G.; Zurakowski, D., *Acta Biomater.* **2018,** *72*, 287-294.
196. FarrokhTakin, E.; Ciofani, G.; Puleo, G. L.; de Vito, G.; Filippeschi, C.; Mazzolai, B.; Piazza, V.; Mattoli, V., *Int. J. Nanomed.* **2013,** *8*, 2319.
197. Wu, M.; Zhang, Z.; Liu, Z.; Zhang, J.; Zhang, Y.; Ding, Y.; Huang, T.; Xiang, D.; Wang, Z.; Dai, Y., *Nano Today* **2021,** *37*, 101104.
198. Shahzad, K.; Mushtaq, S.; Rizwan, M.; Khalid, W.; Atif, M.; Din, F. U.; Ahmad, N.; Abbasi, R.; Ali, Z., *Mater. Sci. Eng. C* **2021,** *119*, 111444.
199. Srinivasa Rao, K.; Hamza, M.; Ashok Kumar, P.; Girija Sravani, K., *Microsyst. Technol.* **2020,** *26* (5), 1671-1679.
200. Ciofani, G.; Danti, S.; D'Alessandro, D.; Moscato, S.; Petrini, M.; Menciassi, A., *Nanoscale Res. Lett.* **2010,** *5* (7), 1093-1101.
201. Janigro, D.; Perju, C.; Fazio, V.; Hallene, K.; Dini, G.; Agarwal, M. K.; Cucullo, L., *BMC Cancer* **2006,** *6*, 72.
202. Marino, A.; Arai, S.; Hou, Y.; Sinibaldi, E.; Pellegrino, M.; Chang, Y. T.; Mazzolai, B.; Mattoli, V.; Suzuki, M.; Ciofani, G., *ACS Nano* **2015,** *9* (7), 7678-89.
203. Marino, A.; Genchi, G. G.; Mattoli, V.; Ciofani, G., *Nano Today* **2017,** *14*, 9-12.
204. Marino, A.; Almici, E.; Migliorin, S.; Tapeinos, C.; Battaglini, M.; Cappello, V.; Marchetti, M.; De Vito, G.; Cicchi, R.; Pavone, F. S., *J. Colloid Interface Sci.* **2019,** *538*, 449-461.
205. FarrokhTakin, E.; Ciofani, G.; Gemmi, M.; Piazza, V.; Mazzolai, B.; Mattoli, V., *Colloids Surf. A: Physicochem. Eng. Aspects* **2012,** *415*, 247-254.
206. Casillas-Popova, S.; Bernad-Bernad, M.; Gracia-Mora, J., *J. Drug Deliv. Sci. Technol.* **2022,** *68*, 103121.
207. Kirson, E. D.; Gurvich, Z.; Schneiderman, R.; Dekel, E.; Itzhaki, A.; Wasserman, Y.; Schatzberger, R.; Palti, Y., *Cancer Res.* **2004,** *64* (9), 3288-3295.
208. Kirson, E. D.; Dbalý, V.; Tovaryš, F.; Vymazal, J.; Soustiel, J. F.; Itzhaki, A.; Mordechovich, D.; Steinberg-Shapira, S.; Gurvich, Z.; Schneiderman, R., *Pro. Nat. Acad. Sci.*

2007, *104* (24), 10152-10157.
209. Yoon, Y. N.; Lee, D.-S.; Park, H. J.; Kim, J.-S., *Sci. Rep.* **2020,** *10* (1), 2560.
210. Fakhar-e-Alam, M.; Saddique, S.; Hossain, N.; Shahzad, A.; Ullah, I.; Sohail, A.; Khan, M. J. I.; Saadullah, M., *J. Cluster Sci.* **2022**.
211. Alfareed, T. M.; Slimani, Y.; Almessiere, M. A.; Shirsath, S. E.; Hassan, M.; Nawaz, M.; Khan, F. A.; Al-Suhaimi, E. A.; Baykal, A., *Ceram. Int.* **2022,** *48* (10), 14640-14651.
212. Wu, C.; Wei, X.; Zhao, K.; Jiang, J.; Jiao, M.; Cheng, J.; Tang, Z.; Guo, Z.; Tang, Y., *Ceram. Int.* **2021,** *47* (12), 17550-17559.
213. Meyers, P. A.; Gorlick, R., *Pediatr. Clin. North Am.* **1997,** *44* (4), 973-989.
214. Hanahan, D.; Weinberg, R. A., *cell* **2011,** *144* (5), 646-674.
215. Steinmann, P.; Walters, D. K.; Arlt, M. J.; Banke, I. J.; Ziegler, U.; Langsam, B.; Arbiser, J.; Muff, R.; Born, W.; Fuchs, B., *Cancer* **2012,** *118* (8), 2117-2127.
216. Xin, Z. F.; Kim, Y. K.; Jung, S. T., *J. Exp. Clinical Cancer Res.* **2009,** *28* (1), 1-8.
217. Tsai, H.-C.; Huang, C.-Y.; Su, H.-L.; Tang, C.-H., *PLoS One* **2014,** *9* (3), e90159.
218. Roussakow, S., *Lancet Oncol.* **2017,** *18* (11), e629.
219. Seifert, G.; Budach, V.; Keilholz, U.; Wust, P.; Eggert, A.; Ghadjar, P., *Radiat. Oncol.* **2016,** *11* (1), 1-7.
220. Sasikala, A. R. K.; Kaliannagounder, V. K.; Alluri, N. R.; Shrestha, B. K.; Kim, S.-J.; Ali-Boucetta, H.; Park, C. H.; Unnithan, A. R., *Nano Energy* **2022,** *96*, 107134.
221. Kumar, A.; Sood, A.; Han, S. S., *Carbohyd. Polym.* **2022,** *277*, 118881.
222. Kumar, A.; Sood, A.; Han, S. S., *J. Mater. Chem. B* **2022,** *10* (15), 2761-2780.
223. Kumar, A.; Han, S. S., *Mater. Sci. Eng. C* **2021,** *128*, 112236.
224. Mohammadinejad, R.; Kumar, A.; Ranjbar-Mohammadi, M.; Ashrafizadeh, M.; Han, S. S.; Khang, G.; Roveimiab, Z., *Polymers* **2020,** *12* (1), 176.
225. Bagchi, A.; Meka, S. R. K.; Rao, B. N.; Chatterjee, K., *Nanotechnology* **2014,** *25* (48), 485101.
226. Teixeira, L.; Crippa, G.; Trabuco, A.; Gimenes, R.; Zaghete, M.; Palioto, D.; De Oliveira, P.; Rosa, A.; Beloti, M., *Acta Biomater.* **2010,** *6* (3), 979-989.
227. Beloti, M. M.; de Oliveira, P. T.; Gimenes, R.; Zaghete, M. A.; Bertolini, M. J.; Rosa, A. L., *J. Biomed. Mater. Res. Part A* **2006,** *79* (2), 282-288.
228. Ciofani, G.; Ricotti, L.; Mattoli, V., *Biomed. Microdevices* **2011,** *13* (2), 255-266.
229. Lopes, H. B.; Santos, T. d. S.; de Oliveira, F. S.; Freitas, G. P.; de Almeida, A. L.;

Gimenes, R.; Rosa, A. L.; Beloti, M. M., *J. Biomater. Appl.* **2014,** *29* (1), 104-112.
230. Scalize, P. H.; Bombonato-Prado, K. F.; de Sousa, L. G.; Rosa, A. L.; Beloti, M. M.; Semprini, M.; Gimenes, R.; de Almeida, A. L.; de Oliveira, F. S.; Hallak Regalo, S. C., *J. Mater. Sci.: Mater. Med.* **2016,** *27* (12), 1-10.
231. Jacob, J.; More, N.; Kalia, K.; Kapusetti, G., *Inflamm. Regen.* **2018,** *38* (1), 1-11.
232. Mindlin, R., *J. Elasticity* **1972,** *2* (4), 217-282.
233. Wu, C.; Tang, Y.; Zhao, K.; Mao, B.; Ru, X., *J. Alloys Compd.* **2020,** *845*, 156301.
234. Jelínek, M.; Vaněk, P.; Tolde, Z.; Buixaderas, E.; Kocourek, T.; Studnička, V.; Drahokoupil, J.; Petzelt, J.; Remsa, J.; Tyunina, M., *Mater. Sci. Eng. C* **2017,** *70*, 334-339.
235. Fan, B.; Guo, Z.; Li, X.; Li, S.; Gao, P.; Xiao, X.; Wu, J.; Shen, C.; Jiao, Y.; Hou, W., *Bioactive Mater.* **2020,** *5* (4), 1087-1101.
236. Ahmadi, N.; Kharaziha, M.; Labbaf, S., *Mater. Chem. Phys.* **2019,** *226*, 263-271.
237. Zheng, T.; Zhao, H.; Huang, Y.; Gao, C.; Zhang, X.; Cai, Q.; Yang, X., *Ceram. Int.* **2021,** *47* (20), 28778-28789.
238. Tariverdian, T.; Behnamghader, A.; Milan, P. B.; Barzegar-Bafrooei, H.; Mozafari, M., *Ceram. Int.* **2019,** *45* (11), 14029-14038.
239. Phromyoo, S.; Lertcumfu, N.; Jaita, P.; Jarupoom, P.; Pengpat, K.; Rujijanagul, G., *Ceram. Int.* **2018,** *44* (3), 2661-2667.
240. Shokrollahi, H.; Salimi, F.; Doostmohammadi, A., *J. Mech. Behavior Biomed. Mater.* **2017,** *74*, 365-370.
241. Draghici, A.-D.; Busuioc, C.; Mocanu, A.; Nicoara, A.-I.; Iordache, F.; Jinga, S.-I., *Mater. Sci. Eng.: C* **2020,** *110*, 110704.
242. Dubey, A. K.; Kakimoto, K.-i., *Mater. Sci. Eng.: C* **2016,** *63*, 211-221.
243. Jiao, H.; Zhao, K.; Bian, T.; Tang, Y., *J. Alloys Compd.* **2017,** *715*, 73-82.
244. Vouilloz, F.; Castro, M. S.; Vargas, G. E.; Gorustovich, A.; Fanovich, M. A., *Ceram. Int.* **2017,** *43* (5), 4212-4221.
245. Zhang, Y.; Chen, L.; Zeng, J.; Zhou, K.; Zhang, D., *Mater. Sci. Eng. C* **2014,** *39*, 143-149.
246. Liu, B.; Chen, L.; Shao, C.; Zhang, F.; Zhou, K.; Cao, J.; Zhang, D., *Mater. Sci. Eng. C* **2016,** *61*, 8-14.
247. Ozcelik, B.; Ergun, C.; Liu, H., *J. Aust. Ceram. Soc.* **2020,** *56* (4), 1197-1216.
248. Ehterami, A.; Kazemi, M.; Nazari, B.; Saraeian, P.; Azami, M., *J. Mech. Behavior*

Biomed. Mater. **2018,** *79*, 195-202.
249. Kemppi, H.; Finnilä, M.; Lorite, G.; Nelo, M.; Juuti, J.; Kokki, M.; Kokki, H.; Räsänen, J.; Mobasheri, A.; Saarakkala, S., *Colloids Surf. B* **2021,** *199*, 111530.
250. GhaedRahmati, H.; Frounchi, M.; Dadbin, S., *Mater. Sci. Eng. B* **2022,** *276*, 115535.
251. Liu, J.; Gu, H.; Liu, Q.; Ren, L.; Li, G., *Mater. Lett.* **2019,** *236*, 686-689.
252. Shuai, C.; Liu, G.; Yang, Y.; Yang, W.; He, C.; Wang, G.; Liu, Z.; Qi, F.; Peng, S., *Colloids Surf. B* **2020,** *185*, 110587.
253. Jacob, J.; More, N.; Mounika, C.; Gondaliya, P.; Kalia, K.; Kapusetti, G., *ACS Applied Bio Mater.* **2019,** *2* (11), 4922-4931.
254. Amaral, D. L.; Zanette, R. S.; Almeida, C. G.; Almeida, L. B.; de Oliveira, L. F.; Marcomini, R. F.; Nogueira, B. V.; Santos, M. O.; Brandão, H. M.; Maranduba, C. M., *Biomed. Mater.* **2019,** *14* (3), 035011.
255. Selvarajan, S.; Alluri, N. R.; Chandrasekhar, A.; Kim, S.-J., *Sens. Actuators B: Chem.* **2016,** *234*, 395-403.
256. Su, Y.; Li, W.; Yuan, L.; Chen, C.; Pan, H.; Xie, G.; Conta, G.; Ferrier, S.; Zhao, X.; Chen, G.; Tai, H.; Jiang, Y.; Chen, J., *Nano Energy* **2021,** *89*, 106321.
257. Zhou, H.; Zhang, Y.; Qiu, Y.; Wu, H.; Qin, W.; Liao, Y.; Yu, Q.; Cheng, H., *Biosens. Bioelectron.* **2020,** *168*, 112569.
258. Xu, Z.; Wan, X.; Mo, X.; Lin, S.; Chen, S.; Chen, J.; Pan, Y.; Zhang, H.; Jin, H.; Duan, J., *Nano Energy* **2021,** *89*, 106450.
259. Ouyang, H.; Li, Z., *Sci. Bull.* **2019,** *64* (21), 1565-1566.
260. Dubey, A. K.; Thrivikraman, G.; Basu, B., *J. Mater. Sci. Mater. Med.* **2015,** *26* (2), 1-11.
261. Zhang, M.; Gao, T.; Wang, J.; Liao, J.; Qiu, Y.; Yang, Q.; Xue, H.; Shi, Z.; Zhao, Y.; Xiong, Z., *Nano Energy* **2015,** *13*, 298-305.
262. Vivekananthan, V.; Chandrasekhar, A.; Alluri, N. R.; Purusothaman, Y.; Kim, W. J.; Kang, C.-N.; Kim, S.-J., *Mater. Lett.* **2019,** *249*, 73-76.
263. Selvarajan, S.; Kim, A.; Song, S. H., *IEEE Access* **2020,** *8*, 68219-68225.
264. Wang, S.; Zhang, L.; Wang, L.; He, Y.; Wu, M., *ACS Appl. Nano Mater.* **2022,** *5* (3), 3352-3360.
265. Feng, G.-H.; Su, P.-C., *J. Micromech. Microeng.* **2021,** *32* (1), 015009.
266. Dhall, A.; Islam, S.; Park, M.; Zhang, Y.; Kim, A.; Hwang, G., *ACS Appl. Mater. Interfaces*

2021, *13* (34), 40379-40391.
267. Charthad, J.; Chang, T. C.; Liu, Z.; Sawaby, A.; Weber, M. J.; Baker, S.; Gore, F.; Felt, S. A.; Arbabian, A., *IEEE Trans. Biomed. Circuits Syst.* **2018,** *12* (2), 257-270.
268. Gupta, A.; Sood, A.; Fuhrer, E.; Djanashvili, K.; Agrawal, G., *ACS Biomater. Sci. Eng.* **2022,** *8* (6), 2281-2306.
269. Zhu, P.; Chen, Y.; Shi, J., *Adv. Mater.* **2020,** *32* (29), 2001976.
270. Staedler, D.; Magouroux, T.; Hadji, R.; Joulaud, C.; Extermann, J.; Schwung, S.; Passemard, S.; Kasparian, C.; Clarke, G.; Gerrmann, M.; Le Dantec, R.; Mugnier, Y.; Rytz, D.; Ciepielewski, D.; Galez, C.; Gerber-Lemaire, S.; Juillerat-Jeanneret, L.; Bonacina, L.; Wolf, J.-P., *ACS Nano* **2012,** *6* (3), 2542-2549.
271. Genchi, G. G.; Ceseracciu, L.; Marino, A.; Labardi, M.; Marras, S.; Pignatelli, F.; Bruschini, L.; Mattoli, V.; Ciofani, G., *Adv. Healthc. Mater.* **2016,** *5* (14), 1808-1820.
272. Choi, H. Y.; Jeong, Y. G., *Compos. B Eng.* **2019,** *168*, 58-65.
273. Briscoe, J.; Dunn, S., *Nano Energy* **2015,** *14*, 15-29.
274. Zhu, R.; Zhang, W.; Yang, R., *Sci. Adv. Mater.* **2012,** *4* (8), 798-804.
275. Güthner, P.; Dransfeld, K., *Appl. Phys. Lett.* **1992,** *61* (9), 1137-1139.
276. Uršič, H.; Prah, U., *Proc. Math. Phys. Eng. Sci.* **2019,** *475* (2223), 20180782.
277. Seol, D.; Kim, B.; Kim, Y., *Curr. Appl. Phys.* **2017,** *17* (5), 661-674.